SECURITY

AD-A215 474

Form Approved
OMB No. 0704-0188

1a. REPORT		1b RESTRICTIVE MARKINGS

2a. SECURITY CLASSIFICATION AUTHORITY
S ELECTE
DEC 0 6 1989 **D**
B

2b. DECLASSIFICATION / DOWNGRADING SCHEDULE

3 DISTRIBUTION / AVAILABILITY OF REPORT
Approved for public release;
distribution unlimited.

4. PERFORMING ORGANIZATION REPORT NUMBER(S)	5. MONITORING ORGANIZATION REPORT NUMBER(S)
	AFOSR·TR· 89-1571

6a. NAME OF PERFORMING ORGANIZATION	6b. OFFICE SYMBOL (If applicable)	7a. NAME OF MONITORING ORGANIZATION
University of Houston Department of Physics		AFOSR

6c. ADDRESS (City, State, and ZIP Code)	7b. ADDRESS (City, State, and ZIP Code)
Houston, Texas 77004	BLDG 410 BAFB DC 20332-6448

8a. NAME OF FUNDING / SPONSORING ORGANIZATION	8b. OFFICE SYMBOL (If applicable)	9 PROCUREMENT INSTRUMENT IDENTIFICATION NUMBER
AFOSR		AFOSR-76-2905

8c. ADDRESS (City, State, and ZIP Code)
BLDG 410
BAFB DC 20332-6448

10 SOURCE OF FUNDING NUMBERS

PROGRAM ELEMENT NO	PROJECT NO.	TASK NO	WORK UNIT ACCESSION NO.
61102F	2312	A1	

11. TITLE (Include Security Classification)

MATHEMATICAL SIMULATION OF THE CARDIOPULMONARY SYSTEM

12. PERSONAL AUTHOR(S)
R. Eugene Collins/ Ray E. Calvert/ Humphrey H. Hardy

13a. TYPE OF REPORT	13b. TIME COVERED	14. DATE OF REPORT (Year, Month, Day)	15. PAGE COUNT
Final	FROM _____ TO _____	December 1979	99

16. SUPPLEMENTARY NOTATION

17. COSATI CODES			18. SUBJECT TERMS (Continue on reverse if necessary and identify by block number)
FIELD	GROUP	SUB-GROUP	

19. ABSTRACT (Continue on reverse if necessary and identify by block number)

Multi-chamber mathematical simulators of the circulatory and pulmonary systems have veen developed. These are capable of examining the effects of whole-body acceleration(WBA) for any body position and a variety of breathing maneuvers. The circulatory model has been used to examine the effects of oscillatory WBA with good correspondence between simulator results and available experimental data. The pulmonary model has been used in an extensive study of effects of sustained WBA on pulmonary mechanics and ventilation and the effectiveness of altering the seatback angle in improving WBA tolerance. It was found that WBA effects on pulmonary function are markedly affected by body angle and the the optimal angle is between 60 and 75 to the effective G axis. The pulmonary and circulartory models are currently being merged to produce a model of the complete circulatory-respiratory system. A bio-feedback model for each system will be incorporated to complete the simulator. During the coming year we hope

20 DISTRIBUTION / AVAILABILITY OF ABSTRACT	21. ABSTRACT SECURITY CLASSIFICATION
☑ UNCLASSIFIED/UNLIMITED ☐ SAME AS RPT ☐ DTIC USERS	unclassified
22a NAME OF RESPONSIBLE INDIVIDUAL	22b TELEPHONE (Include Area Code) 767-5021 / 22c OFFICE SYMBOL NL

DD Form 1473, JUN 86   Previous editions are obsolete.   SECURITY CLASSIFICATION OF THIS PAGE

89 12 05 117

to be able to examine the functioning of the system, especially the delivery
of O_2 to the body tissues under high sustained WBA or in various rapid onset
G-profiles characteristic of aerial compbat aneuvers. As a longer term effort
we will begin examining the effects of WBA on different body types in order
to define the optimum subject for WBA tolerance and the effectiveness of
different breathing maneuvers in relieving the adverse effects of WBA.

FINAL REPORT

GRANT AFOSR-76-2905

December 1979

Mathematical Simulation of

the Cardiopulmonary System

R. Eugene Collins, Pay E. Calvert, and Humphrey H. Hardy
University of Houston, Houston, Texas

Mathematical Simulation of the Cardiopulmonary System

Progress Report, December 1979

The problem of developing a computer simulator for the human cardiopulmonary system has been approached from two directions in the first phase of our project, development of a pulmonary model and development of a circulatory model, each distinct from the other. The second phase of this effort addresses interfacing of these two models into a single functional model and incroporation of simulation of physiologic feed-back and control mechanisms into this model. This report consists of three sections and describes the major progress and results achieved in the first phase of this project.

Summary of Section A

Section A is the text of a paper being submitted for publication which concisely describes the development of the equations for the circulatory model as well as the overall progress made in using this model to examine the effects of Whole Body Acceleration (WBA) on the circulatory system. Greater detail on the development of this model was given in our last annual report.

Summary of Section B

Section B consists of the text of a paper being submitted for publication which describes, in detail, our handling of the pressure-volume relationship describing the elastance of the circulatory elements. The relationship employed is significant in that, though

it is achieved by curve fitting techniques, it not only provides an excellent fit to existing data on circulatory elements, but it is a relationship that has been employed in describing elastance in many other organic tissues and may represent a relationship of much broader applicability.

Summary of Section C

Section C consists of the text of R. E. Calvert's doctoral thesis which includes a description of the overall development of the pulmonary model as well as the major progress made during the last year. An indepth examination of the combined effects of WBA and seatback angle on pulmonary mechanics is presented. A principal finding of this study being the prediction that a seatback angle of between 60° and 75° should be optimal in relieving the adverse effects of WBA on respiration.

A more complete summary of each section may be found in the abstracts preceeding each section.

Phase one of this project is nearly complete and the separate models are functioning and providing interesting results describing their respective systems. Phase two has been initiated during the past year. This phase consists of interfacing the two models and developing the overlaping feedback systems which will describe the functioning of the entire respiratory system. Interfacing of the pulmonary model with the pulmonary circulation portion of the circulatory model has been achieved and some results obtained. (See Section A)

The Circulatory Model

A DIGITAL COMPUTER MODEL OF THE HUMAN

CIRCULATORY SYSTEM*

H. H. Hardy, R. E. Collins, and R. E. Calvert

The University of Houston, Houston, TX 77004

ABSTRACT

A digital, many compartment model of the human circulatory system has been developed which simulates pulsatile blood flow and gas transport and exchange. The model is designed specifically to study short term whole-body acceleration (g_z) encountered in modern aerial combat maneuvers and incorporates a realistic representation of the nonlinear elastic characteristics of circulatory elements and the related pressure dependent flow resistance characteristic of these elements.

The model has been shown to properly simulate human data for passive breathing in a supine subject. The computed carbon dioxide and oxygen partial pressures vary realistically around measured average partial pressures for human subjects. The computed time variation of pressures, circulatory chamber volumes and flow rates match corresponding human data. Under sinusoidal g_z variations, the model predicts realistic variations of volumes, flows and pressures.

INTRODUCTION AND REVIEW OF EXISTING MODELS.

A number of models of the circulatory system in man have been developed. In the late fifties and sixties, great strides were made by many researchers in an effort to model the circulatory system. The analog computer was well developed and provided modeling of heart dynamics, which could then be used as a diagnostic aid. This work reached a peak in 1962 when Circulatory Analog Computers[1] was published from the proceedings of the symposium on the applications of analog computers to the study of the mammalian circulatory system held in the Netherlands on April 19 and 20, 1962. Following this, study turned from the circulation itself to the regulation of the circulation. In 1966, a conference was held on the regulation of the circulation and metabolite transport resulting in the book, Physical Bases of Circulatory Transport: Regulation and Exchange.[2] Since that time research in all three areas (arterial pulse propagation, regulation, and gas exchange) has continued independently.

A summary of some of the circulatory models that have been developed is given in Table I (this model is included in the table for comparison). The table indicates the author, date of publication, in what detail the systemic and pulmonary systems have been divided, to what extent physiologic data has been linearized, and the studies performed with the models. From the table, it can be seen that existing models of the circulatory system can be divided into three distinct categories:

1. Those models containing a pumping heart--these are all analog in nature and include Dick and Rideout,[23] Noordergraaf,[4-7] Beneken,[10-12] Hwang,[14] and Croston.[15]

2. Those models addressing the effect of acceleratory stress--only two are known to the authors: that of Green[18] and that of Boyers.[17]

3. Those models containing gas transport and diffusion--many lung models have some form of circulation, usually this consists only of an influx of veneous blood and an efflux of arterial blood. These are not considered. Those models with a more complete circulatory system include those of Saidel,[21,22] Grodins,[19] and Emery[20].

No model, known to the authors, falls within any two of these categories. The model developed here addresses all three categories and therefore is a more comprehensive model.
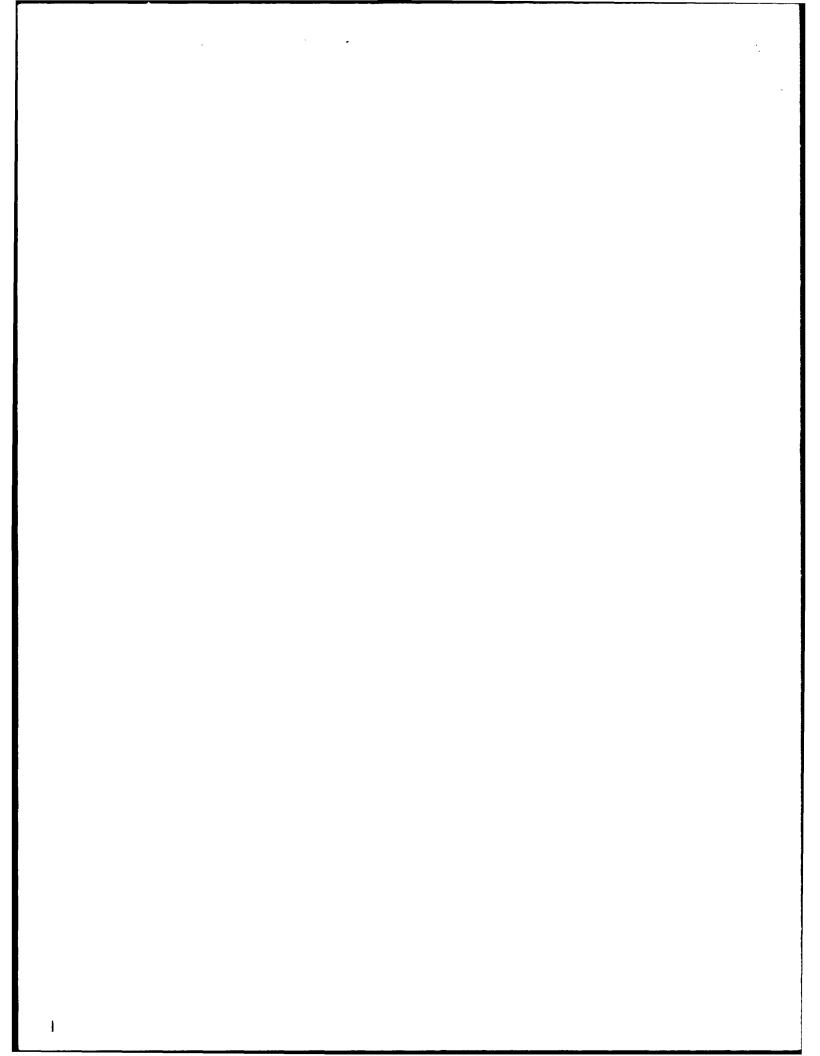
In addition, only one of the models represents flow resistances as dependent on vessel geometry as required by the well-established Poiseuille-Hagen relationship.[24] All but two of the models assume linear pressure-volume or pressure-diameter relationships, yet all in-vivo data and modern in-vitro data (holding vessel length constant) indicate a semi-logarithmic relationship[27-31].

The one model with variable resistance is only an arterial model and is therefore not useful to study the entire circulatory system.   The assumptions made in the remaining models restrict their reliability to small pressure changes and make them of questionable value in studying g-stress.

The model presented here will incorporate better pressure-volume

MODEL AUTHOR	Date(s) of Publication	Only arterial tree	Only systemic circulation	Number of systemic body divisions	Total number of systemic chambers	Number of pulmonary divisions	Linear P-V or P-q	Resistance Independent of Volume	No gas Transport	Constant blood flow assumed	Studies Performed
Green (18)	73		x	1	2	0	x	x	x		g-stress but without a pumping heart
Grodins (19)	67			1	1	1				x	Response to pulsed P_{O_2} and P_{CO_2}. Recovery from Hypoxia. Constant blood flow.
Emery (20)	71			1	1	1				x	Hyperventilation, and breath holding. Constant blood flow.
Saidel (21)	71			0	0	1				x	Nitrogen washout and CO uptake. Constant blood flow.
Saidel (22)	72			0	0	2				x	Sinusoidal breathing with and without obstructive lung disease.
This Model	73			4	12	6					

TABLE 1. Summary of Characteristics of Published Models

and resistance-volume relationships than any complete circulatory model now available in order to make possible a more accurate study of g-stress. In addition, it will include the exchange and transport of gases with a pumping heart.

The model presented here also includes the following anatomical details to simulate further the human circulatory system:

1. Venous return volume has been separated from the capillary volume so that venous storage without significant O_2 and CO_2 exchanges with tissue is possible.

2. Each lung and body compartment has venous return to provide for the gravitational effect of different body orientations and venous storage.

3. The leg return compartment and valves simulate control of circulation, and muscle action on circulation, within the legs.

4. The chest cavity compartment allows changes in blood pressure and flow in response to changes of pleural and alveolar pressure due to breathing.

5. Multiple vascular compartments in the lung will simulate distribution of perfusion and gas exchange with air in the lung.

6. External pressure, P', and resistances at each compartment are variable to simulate short term neural control, g suit effects, and breathing maneuvers.

7. Each portion of the body has a separate control of resistance and compliance allowing simulation of vasoconstriction and dilation in the skeletal muscles while allowing no vasoconstriction in cranial arteries and neither vasoconstriction nor vasodil-

ation in the lungs.

8. A detailed simulation of heart function which permits studies of such abnormalities as a defective heart valve, high blood pressure, or enlarged heart.

9. The variable resistance of the distensible tubes of the vascular system is adequately modeled.

10. The dependence of compartment pressures on gravity and whole body acceleration is included for all body orientations (e.g., horizontal, reclining, legs up, head down, etc.)

BLOOD FLOW EQUATIONS

Here we address the mechanics of blood circulation in the model. The discussion of the blood flow equations is divided into three parts. The first part treats the axial motion of the blood through the blood vessels, the second part treats the transverse motion of blood, vessel wall, and surrounding tissue, and the third part treats the vascular pressure-volume and resistance relationships used in the model.

Throughout the model, the basic assumption is that many branching blood vessels may be approximated by a single vessel of uniform size. Due to the enormous geometric complexity and number of blood vessels in the body, this assumption is essential if a model is to be developed. The single vessel in turn is mathematically equivalent to a capacitive element (henceforth referred to as a vessel or model chamber) and a resistive element (henceforth referred to as a model segment). The combination of the two will be referred to as a model element.

These model elements are linked together to form the entire circulatory model (Figures 1 and 2). Only three types of capacitive elements are employed in the entire model. Type a) consists of a blood volume element able to exchange gases with an alveolar space in the lungs (e.g.: Chamber 5, Fig. 2), b) is a blood vessel able to exchange gas with a tissue volume element (e.g.: Chamber 15, Fig. 1), and c) is a blood volume element having no exchange of gas with exterior elements (e.g.: Chamber 1, Fig. 1). Types a) and b) will be referred to as the capillary elements.

Valves are indicated in Figure 1 within the heart and leg chambers. The flow of blood through the leg, mitral and tricuspid valves is modeled by the specifications such as:

$$\text{if } P_{20} < P_{19}, \ v_{19} \neq 0 \text{ and valve open}$$
(1)
$$\text{if } P_{20} \geq P_{19}, \ v_{19} = 0 \text{ and valve closed}$$

where v_{19} is the volumetric flow rate of blood in ml/sec from chamber 19 into 20, with pressures P_{19} and P_{20} respectively in mm Hg (see Figure 1, legs and leg return). This allows only one-way flow through the leg valves.

The aortic and pulmonary valves also allow only one-way flow, but are modeled in a slightly different way due to inclusion of the inertia of the blood. If the aortic or pulmonary valve is closed, the same conditions apply as in Equation 1. If the valve is open, then the volumetric flow rate is calculated from the equations 3, 5, and 6, and its sign is checked; if positive, calculation continues; if negative, the volumetric flow rate is set to zero, i.e., the valve is closed.
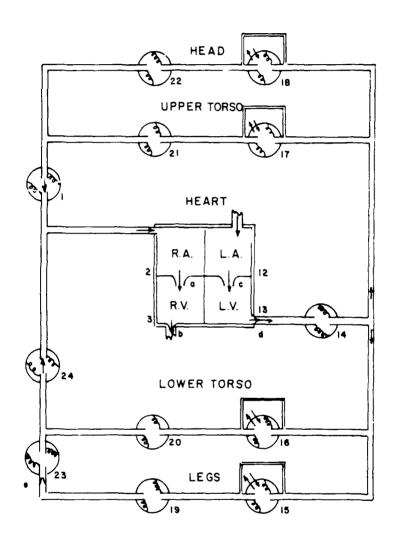
Figure 1. The systemic circulation of the model.
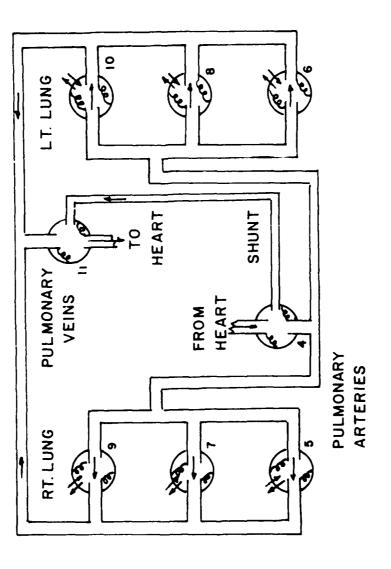
Figure 2. Pulmonary circulation of the model.

AXIAL MOTION

The equations for axial motion of the blood through a circulatory element are derived from momentum conservation, written in terms of forces as source terms. The forces acting consist of the pressure force of the fluid at the inlet, $P_1 A_1$, and the outlet, $-P_2 A_2$, the force of gravity, $\rho g(h_1 - h_2)\bar{A}$, and the viscous drag force at the vessel walls, $-fA_s$ with A_s the surface area of the element. Here A_s is the total surface area of the vessel; $\bar{A}$ is the average cross sectional area of the vessel; $(h_1 - h_2)$ is the distance in cm separating the inlet and outlet ends of the vessel along the direction of the gravitational force; and f is the total drag force per unit area of vessel wall. The algebraic sum of these forces is, according to Newton's second law, a source of momentum in a conservation equation for the axial momentum of the blood in the vessel. In terms of the mean volumetric flow rate through the vessel, q, inlet and outlet rates, q_1, q_2 or velocities, v_1, v_2, and the length of the vessel, L, the equation of motion of the blood is then

$$(2) \quad \frac{d}{dt}(\rho L q) = \rho v_1 q_1 - \rho v_2 q_2 + P_1 A_1 - P_2 A_2 + \rho g(h_1 - h_2)\bar{A} - fA_s$$

Within each model element the axial flow segment is assumed to have a uniform cross sectional area (i.e., $A_1 = A_2 = A$) and constant vessel length, L. The contribution of drag forces, fA_s, can be approximated by $(R'q^2 + Rq) A$ where R' and R are functions of the radius of the vessel[25]. Additional simplifying assumptions are made for each of the model elements. These assumptions are best exhibited if the above equation is written as:

$$(3) \quad \frac{(\rho L)}{A}\frac{dq}{dt} - \rho v_1^2 + \rho v_2^2 + R'q^2 + Rq = P_1 - P_2 + \rho g(h_1 - h_2)$$

This is the equation of axial motion of blood in the model segments connecting left ventricle and aorta and connecting right ventricle and pulmonary artery where the cross sectional area is assumed constant.

In all other model segments, the inertial terms in Equation (3) are considered negligible compared to the drag force term, i.e.,

$$(4) \qquad \frac{(\rho L)}{A}\frac{dq}{dt} - \rho v_1^2 + \rho v_2^2 \ll R'q^2 + Rq$$

This assumption is justifiable since the rate of change of the volumetric fluid velocity is small compared to the rate of volumetric flow under normal conditions. With rapidly changing g, this assumption must be reassessed, but enough information is not yet available for a conclusion at this time. It is also assumed that in these segments, the quadratic term $R'q^2$ is negligible compared to the viscous term Rq. This is reasonable because flow rates are appreciable only between the ventricles and arteries at the peak of systole.[26] These assumptions yield the equation for axial flow in these segments as,

$$(5) \qquad P_1 - P_2 + \rho g(h_1 - h_2) = Rq$$

In addition to the above equations, conservation of mass for an incompressible fluid yields an equation applicable to all of the model chambers for the change of chamber volume $\frac{dV}{dt}$ in terms of the flow into the chamber, v_1, and the flow out of the chamber v_2:

$$(6) \qquad \frac{1}{A}\frac{dV}{dt} = v_1 - v_2 .$$

TRANSVERSE MOTION

The equations for transverse motion of the vessel wall and surrounding tissue are also derived from Newton's second law. The assumption is made that there is no pressure gradient tranverse to the vessel axis within

each of the vessels. An additional assumption of instantaneous equilibrium for the transverse motion of the vessel walls is made. Thus the blood pressure inside the vessel, P, is equal to the external pressure on the vessel and surrounding tissue, P', plus the elastance pressure from the muscular tissue surrounding the vessel, $\bar{P}$, plus a resistive term consisting of a constant, $\bar{R}$, times the rate of change of the volume of the vessel. Thus

$$P = P' + \bar{P} + \bar{R}\,\frac{dV}{dt}$$

(7)

This is the equation used in the model for the transverse motion of the vessel wall and surrounding tissue in the arterial chambers. The assumption of instantaneous equilibrium was made after an in depth computer study which indicated that this assumption affected only the dicrotic notch and had negligible effects (≈ 5 mm Hg) on the rest of the arterial pulse in modeling a passive, supine position.

In order to simplify calculations in the other chambers of the model, the viscous term was considered negligible. The justification for the removal of this term, as with the assumption of instantaneous equilibrium, can only be established by operating the model under various conditions and comparing the results to physiologic data. Other models in which the viscous term was included have demonstrated that $\bar{R}$ is very small, but final acceptance of this approximation will await many computer experiments on the model. With these assumptions, the transverse motion of all other chambers is represented as

(8)

$$P = P' + \bar{P}.$$

THE PRESSURE-VOLUME RELATIONSHIP FOR CIRCULATORY ELEMENTS

As was mentioned in the section on axial motion, the flow resistance factors, R and R', are dependent on the vessel radius, r. In the chambers including the non-linear term in q, however, the cross sectional area of the vessels and therefore the radius of the vessels is assumed constant. Thus R' is a constant for the chambers in the model in which it is not zero . The dependence of R on the vessel radius, however, must be included throughout the model. This is done using the Poiseuille- Hagen formula

(9)
$$R = \frac{\lambda'}{r^4}$$

with λ' a constant. Assuming cylindrical vessel geometry, this formula can be written in terms of the vessel volume,

(10)
$$R = \frac{\lambda}{V^2}$$

with λ a new constant, since vessel length is assumed fixed.

Since the volume of the vessel is a nonlinear function of the transmural pressure, an accurate P-V relationship is essential in setting flow resistances and including g-effects in the model. Using in vivo data from the literature for dogs and man, it was determined that the P-V data for circulatory elements could be fitted more accurately by an equation of the form

(11)
$$V - V_0 = \tau (1 - e^{-k(P_t - P_{t_0})})$$

than by the relationship of Bergel[32] or variations of it presented by other investigators.[27-31] Here (P_{t_0}, V_0) corresponds to any arbitrarily selected Transmural pressure-volume point on the curve, k is a constant characterizing the elastic property of the tissue associated with the

equilibrium is also assumed in the tissue chambers and a uniform gradient is assumed within the vessel walls through which the gases diffuse. This is not the case in the real system of course and some studies have addressed this problem.[33]

Using these assumptions, and the conservation of mass of each gas, the rate of change of the number of moles of each gas within a vessel chamber, dN_g/dt, is equal to the number of moles transferred into the chamber per second by all the blood entering the chamber $(Cq)^{in}$, minus the number of moles transferred out of the chamber per second by all the blood leaving the chamber, $(Cq)^{out}$, minus the rate of diffusion from the chamber into the tissue, $D(P-\bar{P})$:

$$(12) \qquad \frac{dN_g}{dt} = [Cq]^{in} - [Cq]^{out} - D(P - \bar{P})$$

where $\bar{P}$ is the partial pressure of the gas in the tissue or alveoli (in mm Hg) adjacent to the capillary chamber, and P is the partial pressure of the gas in the vessel chamber. D can be related to the diffusion constant, σ, as follows:

$$(13) \qquad D = \frac{\gamma A'\sigma}{\ell}$$

where γ is the ratio of concentration to partial pressure within the tissue, A' is the cross sectional area through which diffusion occurs, and ℓ is the distance over which the diffusion occurs. The volumetric blood flow into and out of every chamber, q, is provided by the portion of the model discussed in the previous section.

The model has been designed to model the transport of any number or kinds of gases transported by the blood. Presently however, only O_2 and CO_2 are included. Although there are a number of variables that affect

circulatory element and τ is a constant proportional to the tissue volume associated with the circulatory element.

Throughout the model the resistance factor, R, is a nonlinear function of the vessel volume (Equation 10). This is in turn a function of the elastic properties of the vessel wall and the transmural pressure across the vessel wall as modeled by Equation 11.
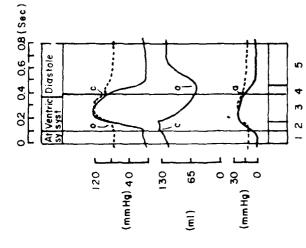
The blood flow equations are solved numerically with the gas transport equations as described in the next section.
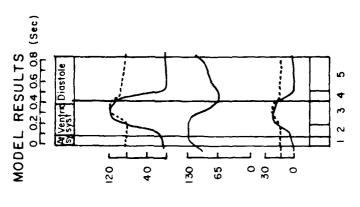
GAS TRANSPORT EQUATIONS

As was illustrated in Figures 2 and 3 the following assumptions are introduced in order to simplify the gas transport portion of the model: Gases enter or leave the circulatory system only by diffusion from the pulmonary capillaries to the alveoli, which lead to the outside air through the airways of the lung, or by diffusion from the capillary beds into body tissues where a loss of oxygen and a gain of carbon dioxide occurs due to tissue metabolism. Throughout the rest of the circulatory system the gases are merely transported, the total number of moles of each gas being conserved. Within each chamber gas may be gained or lost to other chambers by two processes: blood flow or diffusion. Within all but the capillary chambers, the mass of each gas may be increased or decreased only by the influx or efflux of blood containing that gas.

Perfect mixing in every blood and tissue chamber of this model is also assumed. As a consequence, the concentration of each gas in whole blood leaving a chamber is always equal to the concentration of that gas in the chamber. Instantaneous chemical equilibrium is assumed between gases in solution in plasma and bound to hemoglobin within the blood. Instantaneous

Figure 3. Experimental and model results of the left (upper) and Right (lower) ventricular (———) and arterial (––––) pressure changes versus time. Ventricle volume (middle) changes versus time are also shown. Experimental data from Ganong[38].

the number of moles of O_2 and CO_2 in the blood, so far in the model the number of moles of each of these gases is a function of only the partial pressure of both gases and the pH; the pH is in turn considered a function of the partial pressure of both gases.

The number of moles of O_2 in each vessel chamber is calculated as the sum of the number of moles of dissolved O_2 in the plasma, $N_{O_2}^P$, plus the number of moles of O_2 bound to the hemoglobin, $N_{O_2}^h$. The number of moles of O_2 dissolved in the plasma is directly proportional to the partial pressure of oxygen, P_{O_2}, and the volume of plasma, $(1-H)V$, where H is the hematacrit and V is the volume of whole blood:

$$(14) \qquad N_{O_2}^P = \alpha_{O_2} (1-H) V P_{O_2}$$

Here α_{O_2} is the solubility factor.

The number of moles of O_2 bound to the hemoglobin in each chamber, $N_{O_2}^h$, is expressed in terms of the fractional saturation of hemoglobin, S_{O_2}. Since totally saturated blood contains .201 volume percent of O_2 (8.98 moles of O_2 per ml hemoglobin, we have

$$(15) \qquad N_{O_2}^h = S_{O_2} H \beta V$$

where N_{O_2} = number of moles of O_2 in a chamber of blood volume V and

β = 8.98 moles O_2/ml hemoglobin

S_{O_2} = fraction of total O_2 saturation of hemoglobin.

This gives for the total number of moles of O_2 in each chamber, N_{O_2},

$$(16) \qquad N_{O_2} = \alpha_{O_2} (1-H) V P_{O_2} + S_{O_2} H \beta V$$

and for the concentration of O_2,

$$(17) \qquad C_{O_2} = \alpha_{O_2} (1-H) P_{O_2} + S_{O_2} HB$$

Equation 16 becomes, for O_2,

$$(18) \qquad a \frac{dP_{O_2}}{dt} + b \frac{dP_{CO_2}}{dt} = K_{O_2}$$

where $a = \alpha_{O_2} (1-H)V + \beta VH \dfrac{\partial S_{O_2}}{\partial P_{O_2}}$

$$b = \beta \frac{\partial S_{O_2}}{\partial P_{CO_2}} HV$$

and

$$(19) \qquad K_{O_2} = [C_{O_2} q]^{in} - [C_{O_2} q]^{out} - D_{O_2} [P_{O_2} - \bar{P}_{O_2}] - C_{O_2} \frac{dV}{dt}$$

The expression to be used for S_{O_2} is the one given by Gomez[34]. In the process of this calculation, an equation relating pH to the partial pressure of O_2 and CO_2 is required and the one used by Kelman[35] and West[36] was chosen.

In the case of carbon dioxide the gas content of blood was not separated into plasma content and hemoglobin content as was done for oxygen. instead the number of moles, N_{CO_2}, in a chamber is written in terms of the partial pressure of carbon dioxide, P_{CO_2}, the volume of whole blood, V, and a saturation function for whole blood that was adapted from Kelman[35] and West[36], $\bar{S}_{CO_2}$:

$$(20) \qquad N_{CO_2} = \bar{S}_{CO_2} P_{CO_2} V$$

The molecular carbon dioxide concentration is then

$$(21) \qquad C_{CO_2} = \bar{S}_{CO_2} P_{CO_2}$$

and Equation 20 becomes

$$(22) \quad c\,\frac{dP_{O_2}}{dt} + d\,\frac{dP_{CO_2}}{dt} = K_{CO_2}$$

where $c = \dfrac{\partial C_{CO_2}}{\partial P_{O_2}}\,V$

$$d = \frac{\partial C_{CO_2}}{\partial P_{CO_2}}\,V$$

and

$$(23) \quad K_{CO_2} = [C_{CO_2}\,q]^{in} - [C_{CO_2}\,q]^{out} - C_{CO_2}\frac{dV}{dt}$$

Equations 17 and 23 are solved simultaneously yielding

$$(24) \quad \frac{dP_{O_2}}{dt} = \frac{dK_{O_2} - bK_{CO_2}}{ad - bc}$$

$$(25) \quad \frac{dP_{CO_2}}{dt} = \frac{aK_{CO_2} - cK_{O_2}}{ad - bc}$$

Equations 24 and 25 are used to model the gas transport into and out of a model chamber and are coupled to the blood transport equations discussed in the previous section and tissue chamber equations discussed below.

The amount of oxygen and carbon dioxide in each of the tissue chambers is altered by the exchange of each gas with capillary chambers by diffusion and by the disappearance of oxygen and the appearance of carbon dioxide due to tissue metabolism. The tissue chamber equations are therefore

$$(26) \quad \frac{dN_{O_2}}{dt} = +D_{O_2}\,(P_{O_2} - \bar{P}_{O_2}) - M_{O_2}$$

$$(27) \qquad \frac{dN_{CO_2}}{dt} = +D_{CO_2}(P_{CO_2} - \bar{P}_{CO_2}) + M_{CO_2}$$

where N_{O_2} and N_{CO_2} are the number of moles of oxygen and carbon dioxide; and $-M_{O_2}$ and $+M_{CO_2}$ are the rates of disappearance of O_2 and appearance of CO_2, respectively.

In the tissues, the number of moles of each gas is assumed to be proportional to the partial pressure of that gas. This leads to the following tissue equations for O_2 and CO_2 that are used in the model:

$$(28) \qquad a\frac{d\bar{P}_{O_2}}{dt} = +D_{O_2}(P_{O_2} - \bar{P}_{O_2}) - M_{O_2}$$

$$(29) \qquad a\frac{d\bar{P}_{CO_2}}{dt} = +D_{CO_2}(P_{CO_2} - \bar{P}_{CO_2}) + M_{CO_2}$$

with a being $1/RT$, the ratio of mole concentration to partial pressure.

The gas transport equations 24, 25, 28 and 29 are solved numerically with the blood flow equations expressed earlier using Hamming's fourth order predictor-corrector integration with a fourth order Runge-Kutta starting procedure.[37] This formulation consists of 84 coupled, nonlinear, simultaneous, differential equations in its present form (including the transport of only O_2 and CO_2). The initial results are given in the next section for example cases.

RESULTS
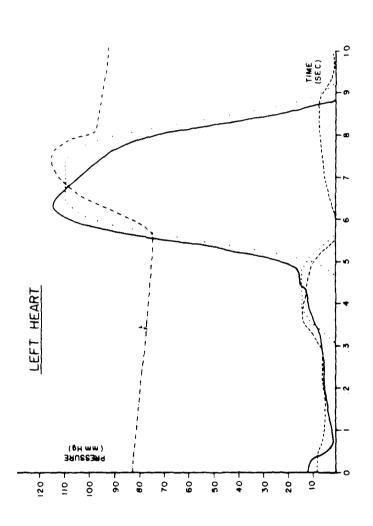
Although the model has been tested for several artificial conditions (constant blood flow with constant alveolar gas pressures, constant blood flow with sinusoidally varying alveolar gas pressures, and a pumping heart with constant alveolar gas pressures), results will be presented in this paper only for the complete model. Specifically, results are presented here for:

the details of the heart pulse, a subject exposed to a sinusoidal variation of G_z, and a supine subject executing passive breathing.

Figure 3 compares the details of physiologic measurements of the heart pulse to model results. The model was run for 6 seconds of real time and the results were plotted for the last second of this period. Only the artifacts (0,C,0',C',a) caused by valve movements are absent in the model results. This is a direct consequence of the omission of tissue inertia as discussed previously. As it is not our purpose to model every detail of heart mechanics, the results given are considered to be in satisfactory agreement with physiologic measurements for proposed applications of the model.

The differences between physiologic values and model values for stroke volume are due to a heart rate of 70 beats/min. in the model while the physiologic measurements were taken at 75 beats/min.

Figure 4 shows the left ventricular pressure on an expanded scale and includes the forcing functions as specified in the model. Left atrial pressure has also been plotted so that the effects of the forcing functions can be seen. These heart pulses were generated without breathing motion of the chest wall and diaphragm but details of the heart pulse, as simulated by the model, are essentially unchanged by passive breathing or by a sinusoidal variation of G_z of amplitude $\pm .5G_z$. This is the case even though breathing does affect blood flows through changes in the pressure within the chest cavity, and hence transmural pressures of circulatory elements, and changing G_z does affect blood pressure throughout the model through the gravity term as discussed previously. These affects are small under these simulated conditions, but will become more significant in

Figure 4. The ventricular pressure (————), aortic pressure (—··—··—), atrium pressure (———), and myocardial muscular pressures (·····) of the Left heart as modeled by the circulatory model.
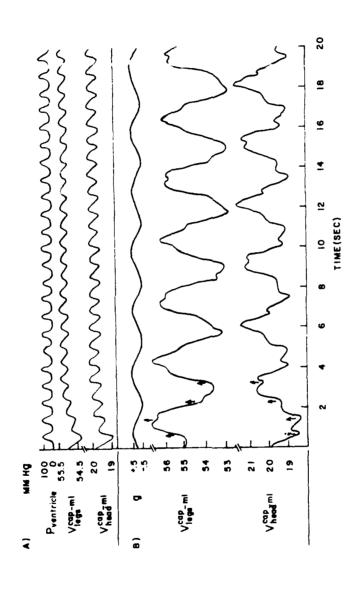
forced breathing and for larger amplitudes of G_z changes.

Model results showing capillary blood volumes for a subject exposed to sinusoidal variation of G_z on the body axis with amplitude 0.5g, with positive acceleration being directed head-to-foot, are given in Figure 5. The capillary blood volumes resulting from the model run without this variation of G are shown for comparison. Notice that the rapid changes in capillary volumes in the upper plots are small, but are clearly the result of the ventricular pressure pulses. A phase shift can be noted between the heart pulse at the ventricle and the volume change at the capillaries. The symbol, ↑, in the figure indicates the time at which the peak of systole is reached. A similar phase shift can be seen in the variation of capillary volumes due to the applied acceleration in the lower portion of Figure 5.
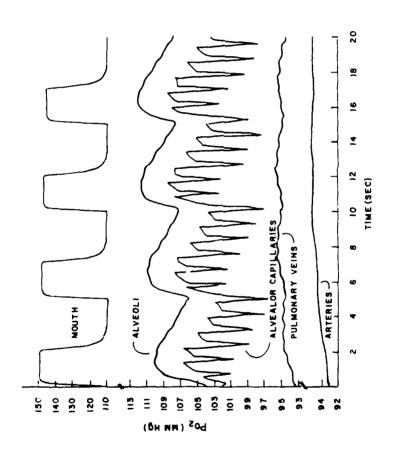
The variations in capillary volume seen here are due to both the variation of G_z and the ventricular pulse. The 180° phase shift between the head and leg capillary volume was to be expected as gravitational forces tend to reduce (increase) the volume of blood in the head at the same time they tend to increase (reduce) the volume of blood in the legs.

Partial pressures in selected chambers of the model are shown in Figures 6 and 7 for a supine subject executing passive breathing. Although the model produces flows, pressures, volumes and gas concentrations for all chambers, as described previously, only the values for a few of the chambers have been selected to be presented here. A number of observations can be made.
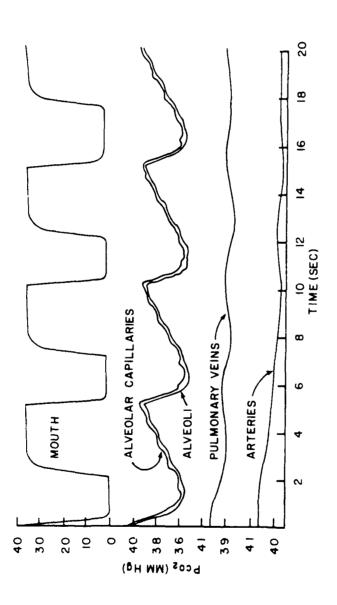
First, the partial pressure of CO_2 in the capillaries is almost identical to that in the alveoli whereas the partial pressure of O_2 in the capillaries is about 7 mm Hg below that in the alveoli. This results because the

Figure 5. Changes in capillary volumes in the head and legs in response to ventricular pressure pulses A) in the supine position ($g_z = 0$) and B) with an imposed sinusoidal variation of g_z ($g_z = +1/2g$). The symbol, ↑, indicates the occurance of the peak of systole.

Figure 6. Partial pressures of oxygen in selected model chambers during
passive breathing when the circulatory model is interfaced with
and existing lung model.

Figure 7. Partial pressures of carbon dioxide in selected model chambers during passive breathing when the circulatory model is interfaced with an existing lung model.

diffusing capacity of CO_2 is twenty times that of O_2 because of the different molecular weights of the molecules.

Secondly, there is a phase difference between changes in partial pressures in alveoli and capillaries for both O_2 and CO_2. This is because it takes some time for the diffusion processes to occur across the vessel walls. The large, periodic drops in the partial pressure of O_2 in the capillaries shown in Figure 6 are a result of the sudden influx of veneous blood resulting from ventricular contractions. This would be reflected in the body as the variation in the distance that capillary blood must travel through the lungs (assuming plug flow) before it becomes fully oxygenated. The fluctuation is much less pronounced in P_{CO_2} as shown in Figure 7 due to the greater diffusion rate of CO_2.

The fluctuations in the partial pressures in the alveolar blood chambers are damped dramatically as the blood moves from one chamber to the next. This effect is due to the assumption of perfect mixing in the model. In fact, by the time the blood reaches the arteries, there is almost no fluctuation in partial pressures. These effects are more pronounced in the model than the real system because perfect mixing does not occur in the real system.

A slight drift is noticeable in the partial pressure of O_2 and CO_2 in the pulmonary veins. This is due to the nonlinear system approaching a slightly different equilibrium under pulsed flow as compared to steady flow. By the end of 20 seconds of real time, however, the drift of values has apparently stopped at new, dynamic equilibrium values. These values are within the range of physiologic measurements as shown in Table II.

SUMMARY AND CONCLUSIONS.

The circulatory model described here appears to be the most complete circulatory model published to date. It has been shown to accurately describe pressures, flows, and volume changes due to heart dynamics in response to a simple applied forcing function simulating contraction of the myocardial muscles (Figure 4 and Appendix). The transport of blood throughout the model subject, produced in this manner, has been shown to respond to small variations in whole body acceleration in a realistic manner. In addition, the circulatory model has been shown to simulate variations of gas concentrations at the mouth, alveolar chambers, and throughout the circulation when interfaced with an existing lung model. Gas exchange and transport has been modeled in such a way that only metabolic rates and gas concentrations need be specified to provide predictions of temporal variation of gas concentrations throughout the body under passive breathing. The detail of direct physiological correspondences included in this cardiopulmonary model make it ideal as a complete experimental subject for physiological studies. Presently the model requires about 25 seconds of CPU time on a Honeywell 6660 to simulate one second of real time but this can be reduced on a faster machine. As was mentioned in the introduction, only the details of the circulatory portion of the cardio-pulmonary model without feedback have been presented in this paper.

The circulatory model has been designed, however, so that feedback mechanisms, external body, forces arbitrary breathing maneuvers, and breathing of different gas mixtures can easily be incorporated. The first stage of this adaption will be to incorporate neural and chemical controls within the model. This is an essential part of a complete circulatory model

as the human circulatory system responds quite differently to stimulus when these controls are blocked as compared to the normal response with feedback. Even so, it is important that a circulatory model simulate supine, resting conditions, even without feedback mechanisms in operation, so that the results of feedback do not mask deficiencies in the primary model. We believe that this has been shown to be the case in the model presented here.

In addition to the incorporation of feedback, the model, as presented here, must be modified slightly to study larger whole body accelerations. The modification must be made as a result of numerical instabilities resulting from the form of Equation 11, which models the pressure-volume relationship in the circulatory elements. This equation predicts an asymptotic volume at infinite pressurization which results in a numerical instability whenever the volume of a circulatory element approaches this asymptotic value. In order to study large and sustained whole body acceleration where some vessels will fill to their maximum capacity, circulatory element volumes in these vessels which approach the asymptotic volumes must be handled in a slightly more complex numerical manner than that presently used. Studies to incorporate this change are underway.

Further studies with the model, that are presently being considered, include: sinusoidal variation of larger amplitude and a variety of frequencies for comparison to experimental data of Dr. C. F. Knapp[41]; linear increases of g to large sustained values for normal subjects and subjects with borderline abnormalities of the cardiopulmonary system; and, ultimately, simulation of g variation encountered in aerial combat maneuvers. Currently a study of alteration of the ventilation-perfusion

distribution in the lungs due to elevated g values is underway. These model studies will complement experimental studies currently in progress at the U. S. Air Force School of Aerospace Medicine. Not only can the model be used for these studies, but it also can be used as a tool to study disease. For example, arterial sclerosis, emphysema and hypertension are only a few of the possibilities.

APPENDIX

Forcing Function Used in the Complete Model in the Heart Chambers

$$FF = Bc^{-A}$$

where B = amplitude of the pulse and

$A = 1/2(t-t_0-a/2)^4/\sigma^2$, $\frac{1}{\delta} > t - t_o > 0$ where δ = pulse rate = 70/sec.

at $t - t_0 = 1/\delta$, t_o reset to $t_0 = t$.

$\sigma = (a/4)^2$

a = pulse duration

t_0 = starting time of the pulse

	t_0 (sec)	a (sec)	(mmHg)
Rt Atrium	.26	.35	5.0
Rt Ventricle	.43	.53	20.0
Lt Atrium	.26	.35	15.0
Lt Ventricle	.43	.53	110.0

REFERENCES

1. Noordergraaf, A., Jager, G. N., and Westerhof, N. Circulatory Analog Computers. North-Holland Publishing Co., Amsterdam, 1963.

2. Reeve, E. G. and Guyton, A. C. Physical Bases of Circulatory Transport: Regulation and Exchange. W. B. Saunders Co., Philadelphia, Pennsylvania, 1967.

3. Beneken, J.E.W. Investigation of the regulatory system of the blood circulation, Circulatory Analog Computers, pp. 16-28, Ed. by Noordergraaf, A., et al., North-Holland Publishing Co., Amsterdam, 1963.

4. Noordergraaf, A. Boom, H.B.K., and Verdouw, P. D. A Human systemic circulatory analog computer, Proc. First Congr. Soc. B.C.G. Res., Zeist, 1960.

5. Noordergraaf, A. Verdouw, P. D., and Boom, H.B.K. The use of an analog computer in a circulation model, Progr. Cardiovase. Dis. 5: 419-439, 1963.

6. Noordergraaf, A. Development of an analog computer of the human circulatory system. In Circulatory Analog Computers, Ed. by Noordergraaf, Amsterdam, North Hall, Publ., 1963.

7. Noordergraaf, A., Verdouw, P. D., van Brummelen, A.G.W., and Wiegel, F.W. Analog of the arterial bed, Pusatile Blood Flow, Ed. by Attinger, E.O., McGraw-Hill, New York, 1964.

8. Robinson, D. A. Ventricular dynamics and tne cardiac representation problem, Circulatory Analog Computers pp. 56-81, Ed. by Noordergraaf, A., et al., North-Holland Publishing Co., Amsterdam, 1963.

9. Defores, J. G., Hara, H. H., Osborn, J. J., and McLeod, J. Theoretical analysis and computer simulation of the circulation with special reference to the Starling properties of ventricles, Circulatory Analog Computers,pp. 91-122, Ed. by Noordergraaf, A., et al., North-Holland Publishing Co., Amsterdam, 1963.

10. Beneken, J.E.W. Electronic analog computer model of the human blood circulation. In Pulsatile Blood Flow. Ed. by E. O. Attinger, New York, McGraw-Hill, 1964, pp. 423-432.

11. Beneken, J.E.W., and Grupping J.C.M. Electronic analog computer model of the human circulatory system. In Medical Electronics. Ed. by F. H. Bostem, Bruxelles, Besoer, 1965.

12. Beneken, J.E.W. and DeWitt B. A physical approach to hemodynamic aspects of the human cardiovascular system. In Physical Bases of Circulatory Transport: Regulation and Exchange. Ed. by Reeve, E. G. and Guyton, Arthur C. W. B. Saunders, 1967, pp. 1-45.

13. Grodins, F.S. and Buoncristiani, J. F. General formulation of the cardiovascular control problem-mathematical models of the mechanical system, Physical Bases of Circulatory Transport: Regulation and Exchange pp. 61-76. Ed. by Reeve, E. B., et al., W. B. Saunders Co., Philadelphia, Penn., 1967.

14. Hwang, N.H.C. and Chao, J. C. An integral form of the hydraulic transmission line equation as applied to circulatory systems, Ninth Annual Sym. on Biomath. Comp. Sci. in Life Series, 1971.

15. Croston, R. C., Rummel, J. A. and Kay, F. J. Computer model fo cardiovascular control system responses toexercise, Journal of Dynamic Systems, Measurement, and Controls, pp. 301-307, 1973.

16.   Attinger. E., Anne, A., Mikami, T., and Sugawara, H. Modeling of pressure-flow relations in arteries and veins, Hemerheology, Ed. by A. L. Copley, Pergamon Press, 1968.

17.   Boyers, D. G., Cuthbertson, J. G., and LUetscher, J. A. Simulation of the human cardiovascular system: a model with normal responses to change of posture, blood loss, transfusion, and autonomic blockage, Simulation, 18:197-205, 1972.

18.   Green, J. F. and Miller, N. C. A model describing the response of the circulatory system to acceleration stress, Annals of Biomedical Engineering, 1:455 - 467, 1973.

19.   Grodins, F. S., Buell, J., and Bart, A. J. Mathematical analysis and digital simulation of the respiratory control system, J. Appl. Physiol., 22 (2): 260-276, 1967.

20.   Energy B., and Pack, A. I. An experimentally verified model of the gas exchanging properties of the lung. Conference on Computers for Analysis and Control in Med. and Biological Research, pp. 130-134, 1971.

21.   Saidel, G. M., Militano, T. C., and Chester, E. H. Pulmonary gas transport characterized by a dynamic model, Resp. Physiol., 12:305 (1971).

22.   Saidel, G. M., Militano, T. C., and Chester, E. H. Mass-balance model of pulmonary oxygen transport, IEEETrans., (BioMed. Engr.) ME19: 205 (1972).

23.   Dick, D. E. and Rideout, V. C. Analog simulation of left heart and arterial dynamics, Proc. 18th ACEMB, Philadelphia, 1965.

24. Skalak, R. Wave propagation in blood flow, Biomechanics, Ed. by Y.C. Fung, ASME, 20-46, 1966.

25. Perry, R. H. and Chilton C. H. Chemical Engineers Handbook. McGraw Hill, New York, 1973.

26. Ruch, T. C. and Patton, H. D. Physiology and Biophysics. W. B. Saunders Co., Philadelphia, Pennsylvania, 1974.

27. Dahn, I., Jonson, B., and Nilson, R. Plethysmographic in vivo determination of the elastic properties of arteries in man, J. Appl. Physiol., 28:328332, 1970.

28. Morris, T. W., Abbrecht, P. H., and Leverett, S. D. Diamater-Pressure Relationships in the Unexposed Femoral Vein, Am. J. Physiol., 227:782788, 1974.

29. Borst, H. G., McGregor, M., Whittengerger, J. L., and Berglund, E. Influence of pulmonary arteral and left atrial pressures on pulmonary vascular resistance, Circulations Res.: 393-399, 1956.

30. Patel, D. J., Greenfield, J. C., and Fry, D. L. in Vivo pressure length-radius relationship of certain blood vessels in man and dog, Pulsatile Blood Flow, pp. 293-305, Ed. by Attinger, E. O., McGraw-Hill, N.Y., 1964.

31. Payne, R.M., Stone, H. L., and Engelken, E. J. Atrial Function During Volume Loading, J. Appl. Physiol. , 31:326-331, 1971.

32. Bergel, E. H. Pulsatile Blood Flow. pp. 275-292, Ed. by Attinger, E. O., McGraw-Hill, N.Y., 1964.

33. Bailey, H. R. Oxygen exchange between capillary and tissue: some equations describing countercurrent and nonlinear transport, Physical Bases of Circulatory Transport: Regulation and Exchange, Ed. by Reeve, E. B. et al., pp. 353-366, W. B. Saunders Co., Philadelphia, Penn, 1967.

34. Gomez, D. M. Considerations of Oxygen-Hemoglobin Equilibrium in the Physiological State, Am. J. Physiol., 49: 105-124, 1965.

35. Kelman, G. R. Digital computer procedure for the conversion of P_{CO} into Blood CO_2 Content, Respir. Physiol., 3: 111-115, 1967.

36. West, J. G. Bioengineering Aspects of the Lung. Marcel Dekker, Inc., N.Y., 1977.

37. Carnahan, B., Luther, H. A. and Wilkes, J. O. Applied Numerical Methods, John Wiley & Sons, Inc., 1969.

38. Ganong, W. F. Review of Medical Physiology. LANGE Medical Publications, Los Altos, CA., 1973.

39. Gordon B. L., et al., ed. Clinical Cardiopulmonary Physiology. Grune & Sratton, Inc., N. Y., 1969.

40. Guyton, A. C. Medical Physiology. W. B. Saunders Co., London, 1971.

41. Knapp, C. F. Response to the cardiovascular system to vibration and conbined stress, Progress Report to Air Force Office of Scientific Research, 1977.

SECTION B

Pressure-Volume Relationship

in Circulatory Elements

ON THE PRESSURE-VOLUME RELATIONSHIP

IN CIRCULATORY ELEMENTS*

H. H. Hardy and R. E. Collins
The University of Houston, Houston, Texas 77004

ABSTRACT

An empirical equation for the in-vivo pressure-volume relationship in circulatory elements is proposed as a universal form valid for all circulatory elements. This equation contains only two fundamental physiologic parameters, one a compliance constant, k, and the other a maximum element volume, V_m. It is suggested that k has the same value for similar elements in all normal individuals and V_m is proportional to total tissue volume of the subject. Fits of this equation to published atrial, ventricular, venous, and arterial data are presented which support these conjectures. Combined with the Poiseulle relationship, this equation is shown to produce a fit to data of flow resistance versus transmural pressure for the pulmonary vascular system of a dog.

ON THE PRESSURE-VOLUME RELATIONSHIP

IN CIRCULATORY ELEMENTS

H. H. Hardy and R. E. Collins
The University of Houston, Houston, Texas 77004

Introduction

Since Bergel[1] first established the nonlinear nature of vessel elastance a number of empirical relationships have been proposed to describe the dependence of blood volume on transmural pressure for circulatory elements. The relationships introduced by Gessner[2] Attinger[3] and Glantz[4] provide good fits to experimental data but both contain a multiplicity of parameters which vary from vessel to vessel with no apparent physiological basis for their choice. Gaasch[5] has proposed the simpler form

$$(1) \qquad\qquad P = be^{kV}$$

to relate transmural pressure, P, to end-diastolic ventricular volume, V, with b and k empirical constants. This relationship requires the assignment of values to only two parameters but, as pointed out by Glantz[4], it is subject to the rather severe criticism of predicting zero blood volume for positive transmural pressure and the fit to data deteriorates as the accuracy of data is improved.

In this brief note we propose a new form of equation to relate transmural pressure and blood volume, valid for all circulatory elements with the possible exception of capillary beds, which is free of these criticisms.

The Proposed Equation

The equation we propose to relate transmural pressure, P, and blood

volume, V, in a circulatory element can be deduced by the following argument: We observe that data of V plotted versus P always indicate a limiting asymptote at a volume, Vm, characteristic of the circulatory element. Thus the derivative

$$(2) \qquad \frac{dV}{dP} = f(V)$$

can be viewed as a function of V which approaches zero at Vm and therefore an expansion of f(V) in a Taylor series in $(V - V_m)$, for $V < V_m$, gives

$$(3) \qquad \frac{dV}{dP} = k(V-V_m) + \text{higher order terms}$$

with k the value of $-df/dV$ at V_m. Then, neglecting terms of higher than first order in $(V-V_m)$

$$(4) \qquad k = \frac{1}{V_m - V} \frac{dV}{dP}$$

defines k as a constant, having dimensions of compliance, characteristic of the circulatory element. Indeed, k characterizes the elastic property of the vessel wall and surrounding tissue while the other parameter in this equation, V_m, represents the limiting volume of the vessel at infinite pressurization.

We note that since the right member of Equation (4) can be multiplied and divided by a scale factor, say α, to define a volume V' as αV having a maximum value V'_m given as αV_m it is reasonable to expect this equation to apply to circulatory elements of different sizes with one value of k applicable to all elements, regardless of size, if these are of the same type.

Data, taken from the literature, appear to support these conjectures. However, before we examine these data we wish to stress the significance of the volume-scale independence already noted in Equation (4). Since all normal individuals of a given specie have sizes, or volumes, of the various elements of

their body in direct proportion to their total mass we expect that the value of V_m, and also V at a given P, should be proportional to the size, or mass of the individual. Indeed such "scaling" of anatomical systems and parameters has been observed to hold, even across species.[6]

The pressure-volume equation implied by Equation (4) is simply obtained by integration as,

$$(5) \qquad P = P_o - \frac{1}{k} \ln \frac{V_m - V}{V_m - V_o}$$

with V_o, P_o being the values of V and P, respectively, at an arbitrary point on the pressure-volume curve. We wish to stress this fact because this equation actually contains only <u>two</u> physiological constants, k and V_m, characteristic of the circulatory elements. We now show how well this equation fits in-vivo data.

Experimental Validation

Figure (1) shows data from Dahn[7] for the pressure-volume relationship in the leg arteries of men. Figure (2) shows these same data normalized on the volume scale by dividing by leg volume and translated vertically on the $V-V_o$ scale to coincide as presented by Dahn. This translation is equivalent to changing the reference point P_o, V_o. Also shown is the fit of Equation (5) to these data. Note that one value of k applies to all three individuals and blood volumes are proportional to total tissue volume.

This equation was also fit to in-vivo data of vessel diameter, D, versus transmural pressure, as shown in Figure (3) using data on dogs from Morris[8], by writing V as $\pi D^2 L/4$ and assuming the length, L, a fixed constant. Again the fit is very good and a single value of k applies to both animals. The scaling of blood volumes by animal size could not be confirmed here because animal sizes were not reported.
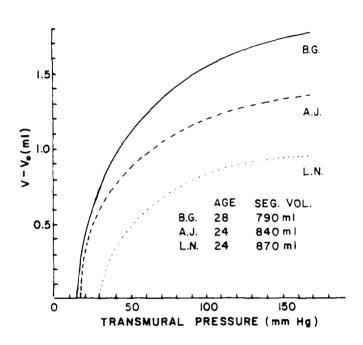
Figure 1. Plethysmographic data from Dahn[7] showing the in-vivo pressure-volume relationship for leg arteries of men.
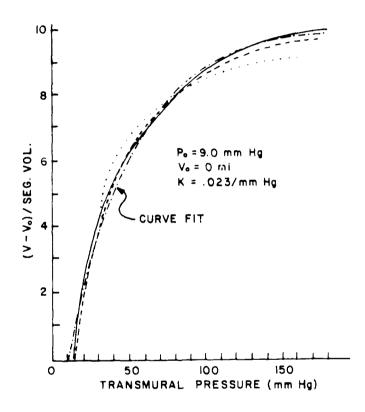
Figure 2. The curves of Figure (1) have been made to coincide by dividing element volumes by tissue segment volume and then translating on the vertical scale. The fit of Equation (5) to the data is shown by the solid curve. The parameter k has the same value for all three subjects.
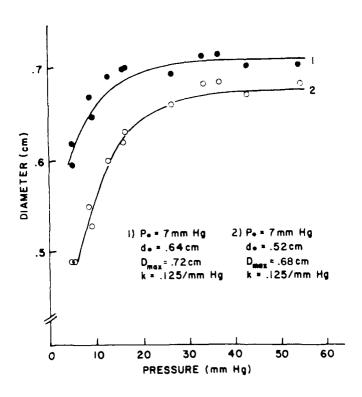
Figure 3. A fit of Equation (5), assuming cylindrical vessel geometry, is shown for data obtained by Morris[8] of the X-ray determined diameter-pressure relationship in the femoral veins of dogs. The parameter k has the same value for both dogs.

Fits of this equation to atrial pressure-volume data were also tested by using data from Payne[9] as shown in Figure (4). This fit to diameter versus pressure was made by assuming a spherical configuration with volume $\pi D^3/6$. Clearly the fit of the equation to data is better than the reproducibility of the data. Here again one value of the compliance constant, k, applies to both subjects. We also fitted this equation to some in-vitro data of ventricular volume versus pressure obtained by Glantz[5] as shown in Figure (5). These data were not very reproducible and the fit of the equation was not as good as for other data, probably because this was not in-vivo data.

As a final example showing validation of the proposed pressure-volume relationship we exhibit the dependence of flow resistance on transmural pressure predicted by this equation and compare it to data. Again assuming the cylindrical volume $\pi D^2 L/4$, with L fixed, for blood volume, we use the Hagen-Poiseuille expression, $\mu L/2\pi D^4$, for flow resistance, R, and our Equation (5) then to relate R to transmural pressure through the dependence of diameter on pressure. The resulting equation can be written as,

$$(6) \qquad R = \frac{\lambda}{V^2}$$

with λ a constant depending on vessel length and blood viscosity and the dependence of V on P given by Equation (5). If Equation (5) is substituted here the result has the form

$$(7) \qquad R = (a - be^{-kP})^{-2}$$

This equation was fitted to data of flow resistance versus transmural pressure for the pulmonary vascular system of dog lungs, as obtained by Borst[10]. This is shown in Figure (6). Clearly the fit is excellant over the entire range of pressure even
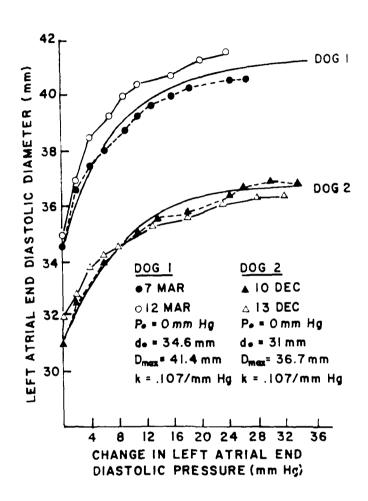
Figure 4. Fits of Equation (5), assuming spherical geometry, to in-vivo end-diastolic atrial pressure–diameter data in dogs obtained by Payne[9] are shown. The parameter k has the same value for both dogs.
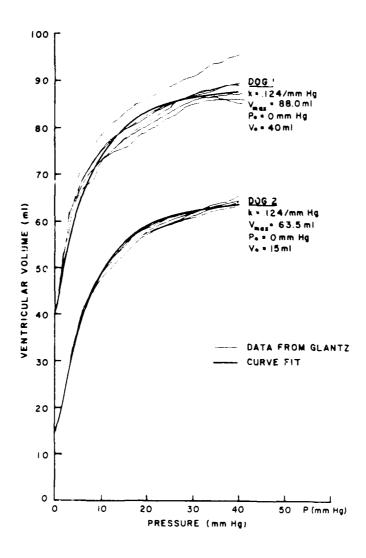
Figure 5. Fits of Equation (5) to in vitro ventricular pressure-volume data of dogs, obtained by Glantz[5], are shown. The parameter k has the same value for both dogs.
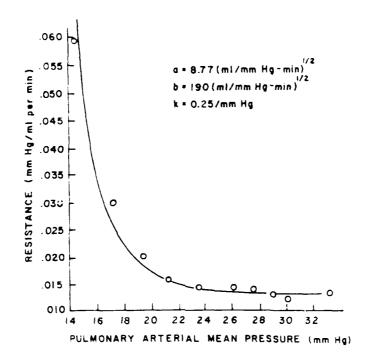
Figure 6. A fit is shown of Equation (7) to data obtained by Borst[10] of flow transmural pressure in the pulmonary vascular system in a dog.

though the pressure flow curve in the lung depends on several physiologic variables (e.g., lung inflation, alvelor pressure, vasomotor tone, etc.). This fit provides further confirmation of the basic validity of Equation (5).

Conclusion

The equation proposed here to describe the pressure-volume relationship of in-vivo circulatory elements has been shown to fit a wide variety of experimental data. Although a direct physiological basis has not yet been established it appears that the two parameters, k and V_m, of the equation are, in fact physiological constants characteristic of circulatory elements and that the value of V_m is scaled by the body size of the subject. It also appears that the value of k may be characteristic of each anatomically distinct type of circulatory element. Indeed it may very well prove possible to distinguish an abnormal circulatory element by the extent to which the k value differs from the universal value characteristic of the element type, but this remains to be demonstrated.

References

1. Bergel, E. H. *Pulsatile Blood Flow.* pp. 275-292, Ed. by Attinger, E. O., McGraw-Hill, N. Y., 1964.

2. Gessner, U. R. S. Wave propagation in Arteries with nonlinear distensibility, *Circulatory Analog Computers,* pp. 82-90, Ed. by Noordergraaf, A., et al., North-Holland Publishing Co., Amsterdam, 1963.

3. Attinger, E., Anne, A., Mikami, T., and Sugawara, H. Modeling of pressure - flow relations in arteries and veins, *Hemerheology,* Ed. by A. L. Copley, Pergamon Press, 1968.

4. Glantz S. A. Ventricular pressure-volume curve indices change with end-diostolic pressure, *Circulation Research,* 39: 772-778, 1976.

5. Gaasch, W. H., Battle, W. D., Oboler, A. A., Banas, J. S., and Levine, H. J. Left ventricular stresses and compliance in man, *Circulation,* XLV: 746-762, 1972.

6. Rashevsky, N. *Mathematical Biophysics.* The University of Chicago Press, Chicago, Illinois, 1948.

7. Dahn, I., Jonson, B., and Nilson, R. Plethysmographic in-vivo determination of the elastic properties of arteries in man, *J. Appl. Physiol.,* 28:328-332, 1970.

8. Morris, T. W., Abbrecht, P. H., and Leverett, S. D. Diameter-Pressure Relationships in the Unexposed Femoral Vein, *Am. J. Physiol.,* 227:782-788, 1974.

9. Payne, R. M., Stone, H. L., and Engelken, E. J. Atrial Function During Volume Loading, *J. Appl. Physiol.,* 31:326-331, 1971.

10. Borst, H. G., McGregor, M., Whittengerger, J. L., and Berglund, E. Influence of pulmonary arterial and left atrial pressures on pulmonary vascular resistance, *Circulations Res.:* 393-399, 1956.

SECTION C

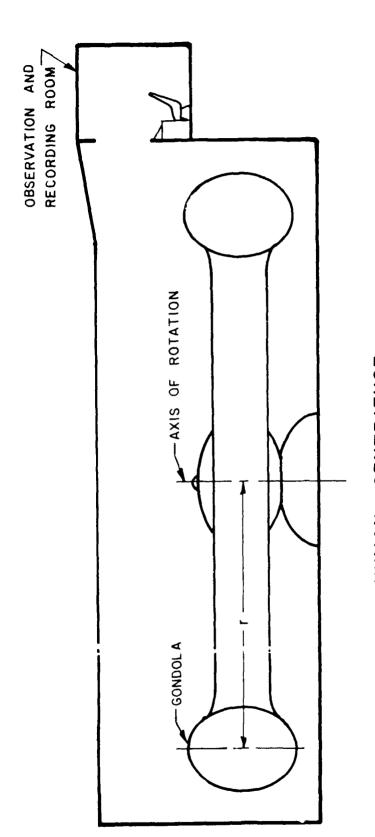The Pulmonary Model

TABLE OF CONTENTS

ABSTRACT

A comprehensive mathematical model of pulmonary mechanics
and regional ventilation is developed and used to examine the
combined effects of high Whole Body Acceleration (WBA) and altered
body position on respiratory mechanics and ventilation. The model
consists of a system of driving pistons representing the respira-
tory muscles, a five chambered bronchial tree, and six parenchyma
chambers. It also simulates gravitational forces on the masses of
the chest, diaphragm and abdomen and resulting effects on fluid
pressures within the chest and abdominal cavities. Furthermore
the model incorporates the effect of the hydrostatic pressure gradient
within the pleural fluid on regional lung volumes for any gravitational
field. The model is shown to be adequate for simulation of many
clinical pulmonary function tests. Several studies are conducted to
determine effects of the high WBA environment on respiration and how
altering body orientation relative to the G field may improve G
tolerance. As a result of these studies, it is concluded that the
optimum seatback angle for maintaining near normal ventilation under
WBA is between 60° and 75°.

I. INTRODUCTION

The effects of artificially altered gravitational forces caused by whole body accelerations (WBA) on the human respiratory system were first recognized as a problem for study shortly after the development of modern aviation. Today, with the advent of high performance aircraft in use by our military, as well as similar planes in use by other countries around the world, this problem has become a critical limiting factor in the training of pilots. While some planes in use today, specifically the F-15, YF-16, and YF-17, have the capability of withstanding up to 16-G maneuvers, a pilot will usually blackout before 12-G's. As has been demonstrated by Burton,[1] even a small advantage in WBA tolerance limits will almost certainly give a pilot the needed superiority during an aerial combat engagement. Consequently, any means of defining the physiological parameters involved in pilot failure and, hopefully, how these might be modified to improve pilot tolerance of WBA, prove to be of scientific interest and in the interest of our national security.

Thus far, the primary tool for investigating the effects of WBA has been the human centrifuge. The history of this device dates back at least to 1815[2] when a centrifuge was used for the treatment of mental patients; however, as pointed out by Gauer[3] in his review of the history of the machine, it had its maximum healing effect only when a second treatment was suggested. The centrifuge consists of a gondola on a long arm which may be spun at controlled speeds. (See Figure 1). WBA is given as multiples of earth normal gravity (G's) and is calculated as
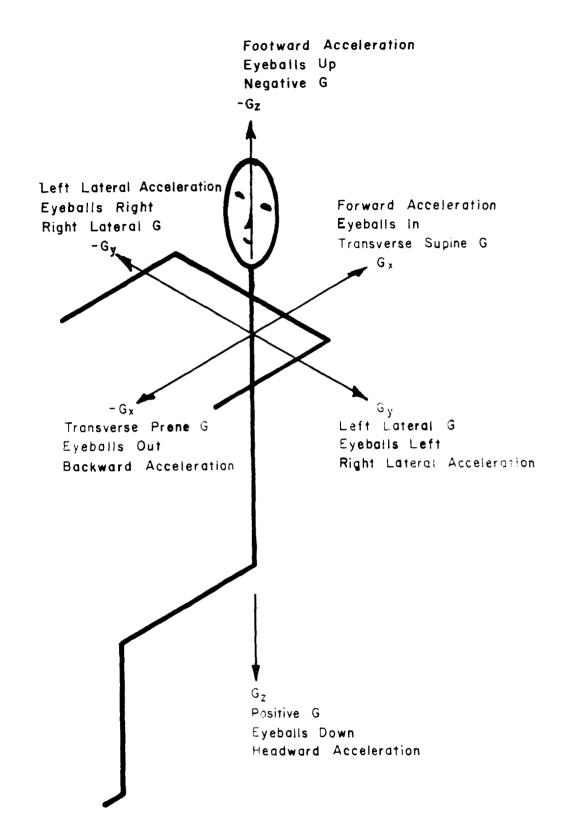
OBSERVATION AND RECORDING ROOM

AXIS OF ROTATION

GONDOLA

r

HUMAN CENTRIFUGE

FIGURE 1

$$\text{(1)} \qquad WBA = \frac{4\pi^2(rps)^2 r}{g}$$

where rps is revolutions per second, r is radius, and g is the gravitational constant. The nomenclature used to define the direction of forces generated are given in terms of body geometry (See Figure 2). The centrifugal field must be summed vectorially with Earth's gravitational field to obtain the resultant field. To eliminate confusion, all future references to WBA will be assumed to refer to the magnitude of the resultant force and direction indicated by degrees off the G_z axis, i.e., G_z is 0°, G_x is 90°, $-G_z$ is 180°, and $-G_x$ is 270°. The axis along the resultant force line will be referred to as the G-axis. Left and right lateral forces will not be examined at this time.

While the centrifuge remains the primary tool used to investigate the effects of WBA, it has many drawbacks and data collected on this device in the study of the pulmonary system is sketchy at best. Many experiments cannot be run on animals as they require cooperation of the subjects. When working with human subjects, for the most part, only noninvasive techniques are allowed. Experimental control is difficult as fatigue sets in rapidly, limiting the data collected on a subject during a single session. Work with human subjects is further complicated by the fact that high WBA studies are always associated with a certain amount of risk and, besides the parameters of interest to the study, many vital signs must be monitored for which medical personnel must be present. It is, therefore, desirable that a good model of the pulmonary system be developed which may be used to direct and augment studies using the human centrifuge.

Footward Acceleration
Eyeballs Up
Negative G

$-G_z$

Left Lateral Acceleration
Eyeballs Right
Right Lateral G

$-G_y$

Forward Acceleration
Eyeballs In
Transverse Supine G

G_x

$-G_x$

Transverse Prone G
Eyeballs Out
Backward Acceleration

G_y

Left Lateral G
Eyeballs Left
Right Lateral Acceleration

G_z
Positive G
Eyeballs Down
Headward Acceleration

WHOLE BODY ACCELERATION NOMENCLATURE

FIGURE 2

Many models of the pulmonary system have been developed in recent years. One of the most frequently encountered is the single chambered model. A very detailed model of this type was developed by Suwa and Bendixin[4] which incorporated diffusion and perfusion. Scheid and Piiper[5] employed such a model to evaluate the effect of respiratory patterns of gas washout data. Among those to apply such a model to the study of lung mechanics are Fry and Hyatt[6] who examined the effects of tissue elastance and pleural pressure on flow resistance in a single airpassage and Collins, et al.,[7] whose model differed from that of Fry and Hyatt in that it incorporated the compliance of the respiratory muscles such that the role of the active components of the ventilation system could be examined. The last two models are among those most firmly based on sound physical principles. Features from each are incorporated into our model as discussed in the next section.

A few multicompartment models have been advanced for the evaluation of ventilation tests. Gomez, et al.,[8,9,10,11] have developed a very sophisticated mathematical treatment of such a model, but it has been criticized for assuming all chambers to be ventilated in parallel.[12] Both Saidel, et al.,[13,14] and West[15,16,17] have developed similar models which included both series and parallel ventilation, which is a more realistic approach, and is incorporated into our model. Their models were designed to study ventilation, however, and do not lend themselves readily to the study of mechanics.

Among those models designed specifically for the study of mechanics are those of Mead, et al.,[18] and Lambert and Wilson,[19] both of which were designed to study elastic characteristics of the lung. Their work may be criticized as the physical laws employed are valid only for small deformations, thus entailing linear theory.

Two other types of model commonly encountered in the literature are (a) those which employ electrical analogs, noteworthy of which are those of Grimby, et al.,[20] and Hilberman, et al.,[21] and (b) those which apply curve fitting techniques to clinical and experimental data and attempt to correlate results with physiologic parameters. The first of these, by virtue of its inherent linearity, can only be addressed to linear portions of lung dynamics which restricts its usefulness to a narrow range around passive breathing. Models of the second type are among those most commonly encountered in the literature; however, they yield virtually no direct information on lung mechanics.

One model of note, which constitutes a separate class, is that advanced by Kilpper[22] in his doctoral dissertation; unfortunately, it has never appeared in public literature. His model consists of a continuous lung tissue system rather than a chambered system. While this model is useful in the study of regional ventilation, it does not incorporate a realistic model of the surrounding tissue.

Though not complete, this list is representative of what has been accomplished in this field. All of these models suffer from one or more of the following restrictions to their usefulness:

i) They rely too heavily on model parameters which are not clearly identifiable with anatomical or physiological elements.

ii) They assume linearity of such parameters as airway resistance or compliance when nonlinearity is known to exist.

iii) They assume that variables such as gas concentrations or alveolar pressures are uniform throughout the system.

As was pointed out by Hyatt and Black[23] in their recent review article, it will not be until an adequate mathematical model of the pulmonary system is developed that the various pulmonary function tests now available can be fully exploited as diagnostic tools. They qualify an "adequate" model as a multichambered model based upon sound physical principles - rather than curve fitting - which incorporates the basic nonlinear nature of the individual pulmonary elements. These comments can be extended to say that if a model is not capable of simulating the various pulmonary function tests, it most certainly will not be of use in examining the effects of WBA.

This dissertation will describe the continued development of a comprehensive numerical simulator of the human pulmonary system first advanced by the author as partial fulfillment of the requirements for the masters degree[24] and its application to specific effects of WBA.

Chapter II will provide a description of the analomical approximations and mathematical relations developed to portray the system. This will be presented much as it was in the above mentioned masters thesis.

Chapters III and IV will describe recent modifications that
have been made to allow the model to depict adequately ˙rway
resistance and lung tissue compliance respectively. Some preliminary
results indicating improved correspondence between model predictions
and observed data are presented in these chapters, the most noteworthy
of which are the pulmonary pressure-volume curve and the graded
effort maximum expiratory flow volume curves.

Chapter V will examine the effect of WBA on the respiratory
system through four studies utilizing the pulmonary simulator, and
Chapter VI will relate these studies to existing knowledge in such
a way that an optimum seatback angle for relieving the adverse effects
of WBA may be defined.

II. THE MODEL

A mathematical model of the human pulmonary system has been developed which incorporates the desirable features of many models previously developed and satisfies the requirements for a model set forth by Hyatt and Black (see page 7). It incorporates the volume dependent nonlinear resistance described by Fry and Hyatt[6], the series and parallel ventilation concept advanced by West[15,16,17] and Saidel, et al.[13,14] and the compliance of respiratory muscles included in Collins' model[7] It also includes several parameters such as the spatial distribution of mass of surrounding deformable tissue and the hydrostatic pressure gradient in the pleural fluid which have been overlooked in previous models, though essential to the study of WBA.
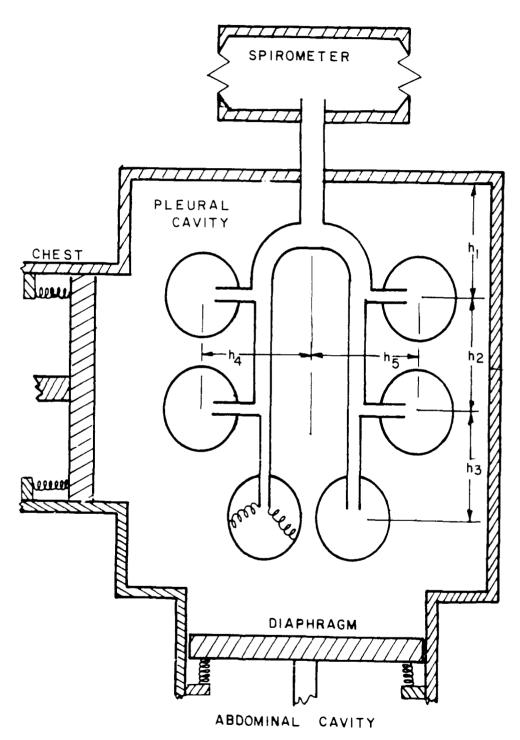
The model advanced by Collins, et al.[7] consists of a single driving piston, representing the muscles of respiration, which acts across a fluid filled pleural space on an alveolar chamber which is connected to the outside of the body via a single elastic passage of the type employed by Fry and Hyatt[6] Though adequate for examining gross lung measurements, such as pulmonary function tests under specific conditions, this model can not be used to explain results in terms of regional characteristics. Further, since all elastic tissues exterior to the lungs were lumped into a single piston, irrespective of geometry, their model proved inadequate in predicting results under changing conditions such as whole body acceleration or changing body orientation with respect to the G-axis.

The respiratory muscles are scattered throughout the trunk
and neck regions of the body and do not act, nor are they acted
upon, by gravity, as a single unit. They should be subdivided into
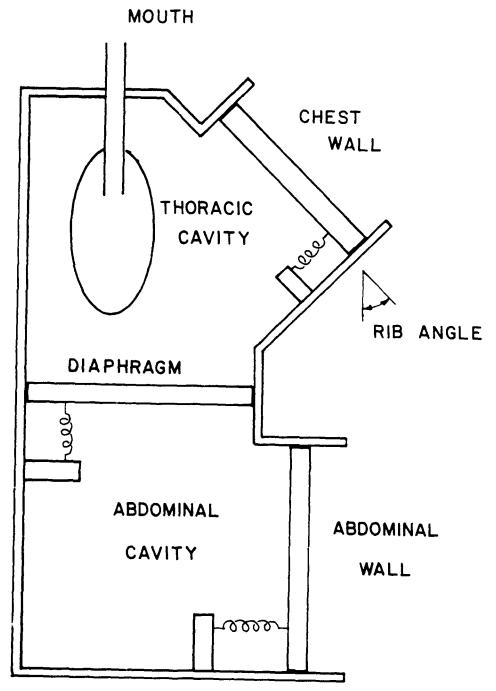a minimum of three anatomical groups, namely:

(1)   thoracic muscles - muscles which act on the rib cage
      and spi.e,

(2)   abdominal muscles, and

(3)   diaphragm muscles.

Lung volume is affected by the weight of each of these groups
according to the architectural design of the human body and its
orientation in the gravitational field. Specifically, lung
volume would be most affected by the mass of the (a) diaphragm
when the G-axis extends through the cephalocaudal axis, G_z axis,
(b) the abdominal muscles when the G-axis passes through the
ventrodorsal axis, G_x axis, and (c) the chest when the G-axis is
perpendicular to the ribs so as to maximize the moment arm of force
on the ribs. Since the diaphragm and abdomen act in series and
since the diaphragm acts only during inspiration while the abdomen
acts only during expiration, these may be thought of as a single
group if the necessary geometry is included to describe the
above mentioned mass distribution effects. This allows the two
piston model depicted in Figure (3) where the geometry of mass
distribution is illustrated in Figure (4).

The lungs are suspended in the thoracic chamber with points of
connection with the rest of the body being only the hilus and
pulmonary ligaments, through which the trachea and pulmonary vessels

SPIROMETER

PLEURAL
CAVITY

CHEST

h_1

h_4 h_5

$h2$

$h3$

DIAPHRAGM

ABDOMINAL CAVITY

LUNG MODEL

FIGURE 3

MOUTH

CHEST WALL

THORACIC CAVITY

RIB ANGLE

DIAPHRAGM

ABDOMINAL CAVITY

ABDOMINAL WALL

GEOMETRIC DISTRIBUTION OF

ACTIVE MUSCLE COMPONENTS

OF THE LUNG

FIGURE 4

pass. It is thus justifiable to treat the lungs as a separate
organ though they cannot function as a separate unit as they
contain no internal driving mechanism, i.e., muscle tissue.[25] The
ventilation portion of this organ consists of (a) an air delivery
system, the conductive zone, and (b) the functional or respiratory
zone.

The conductive zone was extensively examined by Wiebel,[26] who
developed two alternate morphological models of the "respiratory
tree". He meticulously traced and measured branches of this system
in five normal human lungs for the first five branches and
statistically for all remaining branches out to their terminus. His
model A consists of the average values for all measurements for
individual segments of air passages and is characterized as an
irregularly, dichotomously branching system of airways that is
continuous for between sixteen and twenty-five generations of
branches. Model B is a regularly branching air passage system in
which the average measurements for all air passage segments of the
same generation are used. Because of its symmetry, model B is most
often used by mathematical modelers. The model herein developed
does not require symmetry and either of Weibel's models may be
represented.

After an average of nineteen generations, designated as the
trachea, bronchi, bronchioles, and terminal bronchioles respectively
according to their relative depth within the system, the conductive
air passages empty into the acini which consist of the respiratory
bronchioles, alveolar ducts, atrium, and alveolar sacks, all of which

are lined with tiny alveoli. There are within the lungs approximately 300×10^6 alveoli[26] and it is only through the walls of the alveoli that gas exchange between air and blood takes place. The air volume close enough to these specialized structures for mixing and diffusion to bring it into contact with their walls has been designated the parenchyma, the functional unit of which is the acinus.[10,27,28,29] It is the parenchyma which has been designated the alveolar volume of all compartmental models including the one herein advanced. The difference between this volume and the total lung volume is the anatomical dead space[30] and corresponds to the total air passage volume within the model.

The parenchyma may - and has been - subdivided into any number of individual functional units for modeling purposes. In the ideal model this number would correspond to the number of acini in the real lung which would be, since they occur after approximately nineteen branches, 2^{19} or about 5×10^5, which is clearly to large a number for modeling purposes. The field of engineering (a discipline that uses models extensively and from which many of the models of biological systems have come) emphasizes simplicity in modeling and it is upon this rule that the single chambered models are based.

An effect which cannot be examined with a single chambered model and which has not been included in any multichambered model, to the knowledge of this investigator, is that of the pleural pressure gradient in the thoracic cavity. Given the pleural pressure at the top of the lungs with respect to the G-axis, P_{pl_0}, the pleural pressure at any depth, h, along the G-axis may be expressed as

(2)
$$P_{pl} = P_{pl_0} + qgh \ ,$$

where q is the mass density of lung tissue and g is the gravitational acceleration.

The effect of this pressure gradient on the lungs was clearly demonstrated by Glazier, et al.;[31] in his examination of greyhound lungs that were fixed in situ. He found that apical and basal alveoli were the same size when fixed in the same horizontal plane, while apical alveoli were four times larger than basal alveoli when the lungs were fixed vertically. This gradient in unit volume has been attributed to the geometric mass distribution around the lungs and the hydrostatic pressure gradient in the pleural fluid.[32,33,34]

The parenchyma has been subdivided within the model (see Figures (3) and (5)) into six chambers arranged three to a side and spaced at distances h_1, h_2, and h_3 along the cephalocaudal axis and h_4 and h_5 along the right to left axis in the coronal plane. The symmetry imposed by this geometry tends to simplify the examination of the effects of the hydrostatic gradient mentioned above by subdividing each side of the lung into hydrostatic levels, thus allowing the simulation of any body orientation with respect to the G-axis.

It should be noted that this breakdown is purely artificial and bears no relation to the five lobular sections of the lungs. Strict adherence to anatomical structure may be imposed by effectively eliminating one alveolar segment on the left by setting its volume to zero and the resistance into it to infinity and adjusting the size and relative location of the other chambers to a geometry matching the true anatomical state.
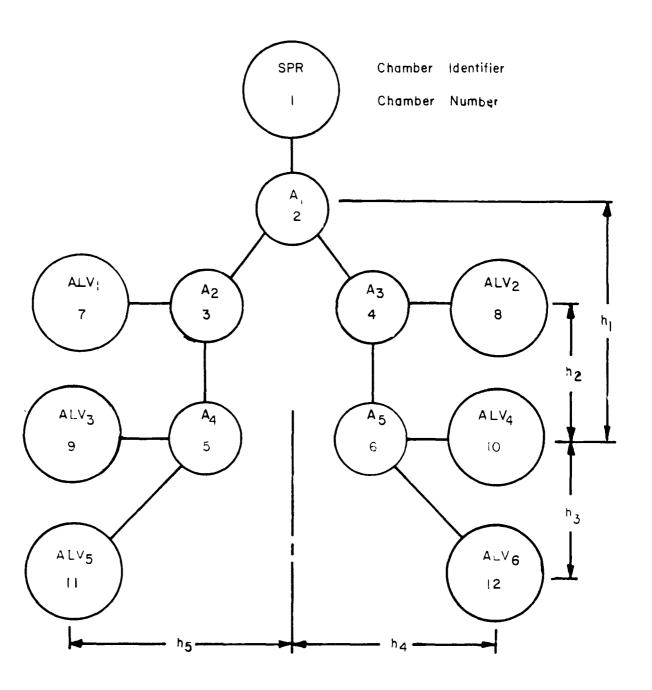
AIR CHAMBERS

FIGURE 5

The airpassages have been subdivided into a system of five bifurcating air chambers allowing both series and parallel ventilation of the six alveolar chambers as indicated in Figures (3) and (5). Within the framework of Weibel's models, Chamber A_1 in Figure (5) corresponds to the nasal or oral cavities, larnyx, trachea, and primary bronchi. Chambers A_2 and A_3 correspond to all secondary and possibly tertiary bronchi in the lungs and all lower order bronchi and bronchioles supplying the upper third of the lungs. Chambers A_4 and A_5 would then correspond to all lower order bronchi and bronchioles supplying the lower two-thirds of the lungs.

Measurements of in vivo human lung volume cannot be made internal to the lungs but are generally accomplished indirectly by a family of instruments called spirometers.[30] While these vary greatly in design they all serve the same basic purpose - to measure the volume of air inspired and expired by the subject during various breathing maneuvers. Chamber Spr in Figure (4), which completes the gas volume portion of the model, represents just such a device. When the initial volume of this chamber is set to a relatively small value (but larger than the volume that can be inspired by the lungs) it represents an ideal spirometer, meaning that it is frictionless and operates at constant pressure and temperature. If the volume of this chamber is set to a very large value it simply represents the atmosphere. Source-sink relations for individual gasses are included within this chamber such that it can be used to model specialized life support systems such as are found in a pilot's cockpit or a diving sphere.

One assumption has been made with regard to the air chambers to simplify the mathematics involved which requires some clarification; all air chambers in the model are considered "ideal mixing" chambers. This concept will be explained for the airpassages and the explanation may be extended to the other chambers. When air (or fluid) passes through a tube it travels not as a square wave (plug flow) pushing all old air in front of the new, but as a paraboloidal front where velocity is greatest at the center and may be zero near the walls. This means that the composition of air near the wall will closely resemble that of the old resident gas while air near the center will reflect that of the inflowing gas. This analogy becomes somewhat muddled around points of high resistance where turbulence may occur, but the message is the same - composition of air within a chamber must be represented as some average of resident and inflowing gas. This concept has been well developed by Pedley, et al.[35] The assumption herein applied is that incoming gas instantly mixes with all resident gas. Considering that instantly here means within one finite integration step (0.01 - 0.001 sec), that the volumes of the chambers are only 0.05 - 0.20 L, and that the flow rate may exceed 1100 L/min., this is a safe assumption.

The development of the equations describing this system starts with the assumption that the volume of the thoracic cavity is equal to the air volume plus a constant, K, which is the volume of pleural fluid and the volume of lung tissue, i.e.,

$$(3) \qquad V_{Tx} + V_{DA} = \sum_{j=1}^{6} V_j + K$$

where V_{Tx} is the volume contribution of the thorax, V_{DA} is the volume contribution of the diaphragm-abdomen complex, and V_j for $j=1$ to 6 are the six alveolar chamber volumes.

The force balance equations describing the pressures acting across the muscle and parenchyma chamber walls (see Figure 6) were developed from Newton's second law. Assuming the inertial terms to be negligible, the force balance equations are:

$$(4) \qquad P_{Tx} + P_{bs} = P_{pl} + \bar{P}_g + P_{el_{Tx}}$$

for the thorax,

$$(5) \qquad P_{DA} + P_{bs} = P_{pl} + P_{g_b} + P_{g_{AB}} + P_{el_{DA}}$$

for the diaphragm-abdomen complex, and

$$(6) \qquad P_j = P_{pl} + P_{g_j} + P_{el_j}$$

for each of the six alveolar chambers, $j = 1$ to 6.

Equations describing the volume dependence of the elastic terms, P_{el}, will be discussed in a later chapter. The basic equatic of pulmonary statics as described by the model are completc when the force balance equations (Equations 4-6) and the conservation of pulmonary volume equation (Equation 3) are coupled with the equation of state for the gas in each chamber, i.e., assuming isothermal conditions,
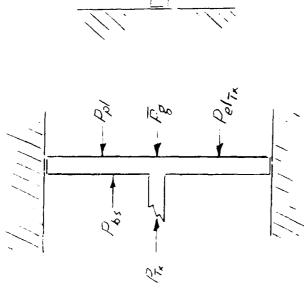
$$(7) \qquad P_j V_j = n_j R T_j$$

FIGURE 6-a
FORCES ACTING ON
THORAX WALLS

P_{bs} = Body surface pressure

P_{Tx} = Driving function for thoracic muscles

P_{pl} = Pleural P at top of cavity (neglecting hydrostatic effects)

$\bar{P}_g$ = Average hydrostic P

$P_{el_{Tx}}$ = P due to elastic components of chest wall
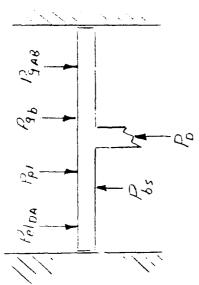
FIGURE 6-b
FORCES ACTING ON
DIAPHRAGM-ABDOMEN WALLS

$P_{el_{DA}}$ = Pel of diaphragm and abdominal walls

P_{g_b} = Hydrostatic P at bottom of thoracic cavity

$P_{g_{AB}}$ = Average hydrostatic P in abdominal cavity

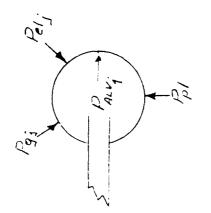P_D = Driving function representing diaphragm-abdominal muscles

FIGURE 6-c
FORCES ACTING ON
ALVEOLAR WALLS

P_{alv_j} = Gas pressure in alveolar cavity

P_{g_j} = local hydrostatic P

P_{el_j} = lung tissue Pel

where n is the total moles of gas, R is the ideal gas constant, and T is temperature.

Two additional equations are necessary to describe pulmonary dynamics; a mass balance equation describing the gas in each chamber and a flow equation describing the transfer of gases between chambers. The latter of these will be treated in a later chapter on airway resistance. If the initial concentration of gas 1 in chamber j is known, the moles of gas present, n_{1j}, may be determined by

(8) $$n_{1j} = n_{0_{1j}} + \int \frac{dn_{1j}}{dt} \, dt$$

where $n_{0_{1j}}$ is the initial value of n_{1j} and

(9) $$\frac{dn_{1j}}{dt} = \sum_i C_{1i} F_{ij} - C_{1j} \sum_k F_{jk} + Diff_{1j}$$

where i is any chamber having flow into Chamber j, k is any chamber into which flow in passing from j, F_{ij} is the volume flow rate from i to j, and C_{1i} is the molar concentration of gas 1 in chamber i, $Diff_j$ is a function representing gas exchange with the blood and would only appear in the alveolar equations.

The complete set of equations consisting of the derivative of the volume equation (Equation 3), the force balance equations (Equations 4-6), the equation of state (Equation 7), and the mass balance equations (Equation 8) for each chamber and each gas as required, constitutes a set of 150 simultaneous, nonlinear differential equations. (For derivation see Appendix A.) These are listed in Tables I, II, and III. The only equations listed

ALVEOLAR EQUATIONS

Eq. No.[*]	Equation

1-6

$$\dot{V}_j = \frac{\frac{\dot{n}RT}{V_j} + \frac{\partial P_{el}}{\partial V_{Tx}} \cdot \dot{V}_{Tx} - \left(\dot{P}_{Tx} + \dot{z}_{os} - \frac{\dot{z}}{z} + \dot{z}_{Ej}\right)}{\frac{\dot{P}_j}{V_j} + \frac{\partial P_{el}}{\partial V_j}}$$

7

$$\dot{V}_{Tx} = \frac{\frac{\partial P_{el\,DA}}{\partial V_{DA}} \sum_j \frac{\dot{V}_j}{z} + \dot{P}_{Tx} - \dot{P}_u - \dot{P}_{ENE} + \dot{P}_{Pl} - \dot{P}_z}{\frac{\partial P_{el\,DA}}{\partial V_{DA}} + \frac{\partial P_{el\,Tx}}{\partial V_{Tx}}}$$

8-31

$$\dot{n}_{kj} = C_{km} F_{kj} - Diff_{kj} \quad [**]$$

32-37

$$\dot{n}_{wj} = V_j \frac{\partial C_{wj}}{\partial P_j} \dot{P}_j + C_{wj} \dot{V}_j$$

38-61

$$\dot{C}_{kj} = \frac{1}{V_j}\left(\dot{n}_{kj} - C_{kj} \dot{V}_j\right)$$

62-67

$$\dot{C}_{wj} = \frac{\partial C_{wj}}{\partial P_j} \dot{P}_j$$

68-73

$$\dot{P}_j = \frac{RT}{V_j}\left[\dot{n}_{wj} + \dot{n}_{Tj} - \dot{V}_j\left(C_{wj} + C_{Tj}\right)\right]$$

74-79

$$\dot{S}_{wj} = \dot{n}_{wj} - C_{wm} F_{kj}$$

[*] Equations are numbered cumulatively based upon the chamber number
    j= 7-12 and gas number 1= 1-4.

[**]See Appendix A for definition of m. Roughly, it is the chamber from
    which gas is flowing.

TABLE I

TRACHEO-BRONCHIAL EQUATIONS

Eq. No. [*]	Equation

1-20
$$\dot{n}_{\ell j} = \sum_i C_i F_{ij} - C_j \sum_k F_{jk}$$

21-40
$$\dot{C}_{\ell j} = \frac{\dot{n}_{\ell j}}{V_j}$$

41-45
$$\dot{P}_j = \frac{\sum_\ell \dot{n}_{\ell j}}{\left(\frac{1}{RT} - \frac{\partial C_{wj}}{\partial P_j}\right) V_j}$$

46-50
$$\dot{C}_{wj} = \frac{\partial C_{wj}}{\partial P_j} \dot{P}_j$$

51-55
$$\dot{n}_{wj} = V_j \dot{C}_{wj}$$

56-60
$$\dot{S}_{wj} = \dot{n}_{wj} - \left[\sum_i C_i F_{ij} - C_j \sum_k F_{jk} \right]$$

* Equations are numbered cumulatively based upon the chamber number
   j= 2-5 and gas number l= 1-4

TABLE II

SPIROMETER EQUATIONS

Eq. No.	Equation
1-4	$\dot{n}_{\ell 1} = - C_{\ell m} F_{12}$
5	$\dot{V}_1 = \dfrac{\sum\limits_{\ell} \dot{n}_{\ell 1}}{\dfrac{P_1}{RT} - C_{w_1}}$
6	$\dot{n}_{w1} = C_{w_1} \dot{V}_1$
7-10	$\dot{C}_{\ell 1} = \dfrac{1}{V_1} \left(\dot{n}_{\ell 1} - C_{\ell 1} \dot{V}_1 \right)$
11	$\dot{S}_{w1} = \dot{n}_{w1} - C_{wm} F_{12}$

TABLE III

which have not been discussed thus far are those for the molar

water concentration, C_{w_j}, the moles of water in a chamber, n_{w_j},

and the source term for water vapor, S_{w_j}. Since water vapor,

unlike the other gases present, has a saturation point dependent

on the P and T of the chamber, a source term must be supplied

in the mass balance equation for water to allow for evaporation

and condensation. For simplicity all chambers in the model are

assumed to be at the saturation point at all times.

The equations in these three tables constitute the complete

set of differential equations required to describe the dynamics of

this model. These were algebraically rearranged such that they

could be sequentially solved (see Appendix A) and were programmed

for numerical integration on a high speed Computer in Fortran IV

language.

The model is always initialized in the relaxed state where

P_{Tx} and P_{DA} are both zero. In this state the system will take

on its equilibrium volume, which is the functional residual

capacity (FRC), and all pressures within the closed air system will

equal P_{spr}. P_{spr} and P_{bs} must be specified constants or time

dependent functions representing the environmental conditions being

modeled. Given the initial gravitational acceleration and its

orientation with respect to the body coronal plane, all hydrostatic

pressures in the pleural space may be calculated using Equation (2)

and pressures due to the weight of each muscle group may be calculated

from input parameters related to the mass of the structure and the

area over which it operates. P_{AB} may be calculated from an equation similar to Equation (2). Since the elastic pressures are modeled as functions only of volume, Equations (3-6) constitute a set of nine equations in nine unknowns, namely: V_{DA}, V_{Tx}, P_{pl}, and V_j for $j = 1-6$.

To solve this set of equations for initial values of the dependent variables listed above a Newton-Raphson iteration was first tried. The equations proved to be very oscillatory, however, and convergence could not be achieved. The modified Newton-Rapson iteration procedure advanced by R. P. Donachi,[36] in which original estimates are corrected by only half the calculated correction values, was attempted but it was found that either convergence was too slow or the system would converge to a constant error. We further modified Donachi's method by using the full correction value if the calculated error for any variable did not change sign during three consecutive iterations, returning to the half step any time sign change was noted. This allowed convergence within an acceptable number of iterations.

A fourth order Hamming predictor-corrector algorithm using a fourth order Runge-Kutta starting procedure[37] was chosen as ~ integration technique; however, upon attempting to run the mouel instabilities were indicated. After performing a stability analysis[37,38] it was found that the pressure equations in the airways were absolutely unstable and the problem could not be corrected using the equations as formulated.

To correct this problem we assumed a steady state distribution
of pressures in the airways; that is, the pressures within the
airway chambers are assumed to readjust instantaneously to changes
in pressures in the alveolar chambers such that no net change in
air mass occurs within the airways. This assumption is justified
because the pressure front due to a change in pressure at any point
in the system travels to other points at the speed of sound although
mass transport occurs at the speed of flow caused by the
instantaneous pressure gradient. Since no point in the system is
much over 1.5 feet away from any other point and the speed of sound
is 1090 ft/sec it is reasonable to assume that pressure will have
redistributed within 0.0015 sec. If the time step, Δt, is larger
than this value the steady state assumption will be not only adequate
but necessary. The modified Newton-Raphson iteration described
earlier was employed to solve the steady state equations for the
pressures within the airways and proved to be very satisfactory.

Two other stability criteria must be imposed on the integration
procedure, namely:

(10) $$\Delta t < \left| \frac{V}{F} \right|,$$

and

(11) $$\Delta t < RC \ .$$

Equation (10) simply states that a chamber must not empty before
incoming gas has had a chance to mix with resident gas and Equation (11)
is just the resistance-compliance criterion imposed upon any
resistor-capacitor system. These conditions allow operation of the
model within a range of Δt greater than 0.002 sec. for forced breathing
and less than 0.025 sec. for passive breathing.

The results of passive breathing simulation, once all parameter values have been set, are given in Figure (7). This figure shows simultaneous values for average alveolar pressure, P_{alv}, driving pressures, P_{Tx} and P_{DA}, total resistance, R, volume flow rate at the spirometer, F, volume changes as measured by the spirometer, V_{spr}, and volume changes of alveolar chambers at each of the three hydrostatic levels. It should be noted that the beginning volumes of the alveolar chambers are not the same. This run was made simulating the vertical sitting position; thus, the different alveolar-FRC volumes reflect unit volume gradient due to gravitational effects mentioned earlier.

The driving pressure equation used was a simple exponential function,

$$(12) \qquad P = (P_{max} - P_{min}) \frac{(1 - e^{-ty})}{(1 - e^{-t_{max}y})}$$

as represented in Figure (7) where $(P_{max} - P_{min})$ represents the range over which the driving pressure will operate, t is the elapsed time during the breathing phase (inspiration or expiration), t_{max} is the phase period, and y is a constant related to the strength of contraction which determines the rate at which contraction takes place. P_{max} and P_{min}, being the end points of inspiration and expiration, may be initially estimated by knowing the desired volume change and using a procedure similar to that used to calculate FRC, assuming that equilibrium will be approached and all gas chamber pressures will be near atmospheric. If equilibrium will not be approached during the run P_{max} and P_{min} will have to be stipulated and experimentally determined.
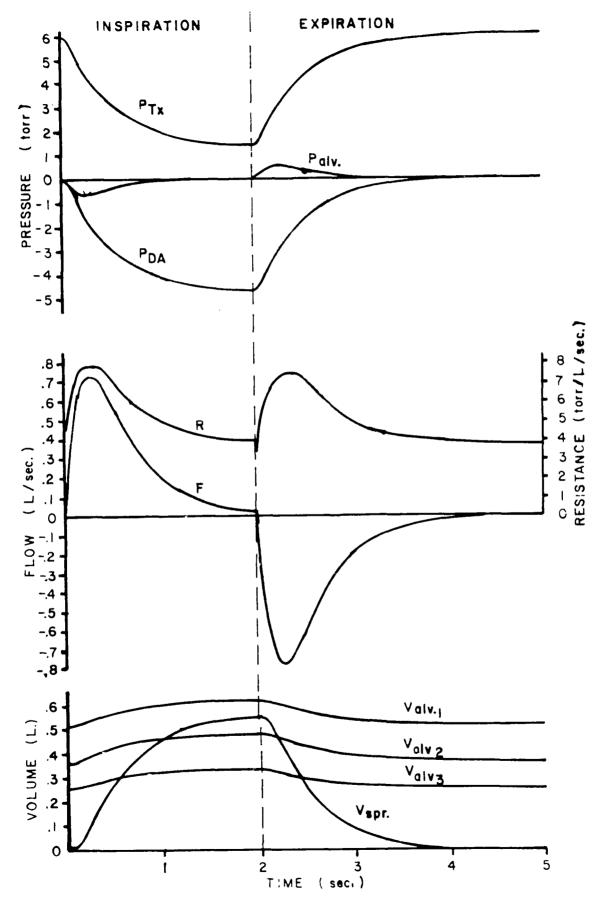
FIGURE 7

It was hoped that by adjusting y, P_{max}, and P_{min} it would be possible to simulate any breathing maneuver. When forced breathing simulation was attempted, however, Equation (12) failed, yielding a peak expiratory flow rate far too low, or reaching total lung capacity (TLC) far too soon. This problem will be discussed more fully in the next two chapters.

III. RESISTANCE

Classically, airway resistance has been expressed as

(13) $$\Delta P = R\dot{V}$$

where ΔP is the pressure difference between the lungs and the mouth, R is resistance, and $\dot{V}$ is volume flow rate. This, of course, is the equation for laminar flow through a rigid tube. As early as 1915, however, Rohrer[39,40,41], who was the first to apply fluid dynamics to the study of lung mechanics, noted that pressure-flow data was not linear, but could better be represented by the quadratic

(14) $$\Delta P = K_1\dot{V} + K_2\dot{V}^2$$

where K_1 and K_2 are constants characteristic of the data set. This relation, though empirical in nature, may be derived from fluid mechanics if several simplifying assumptions are made[42]. An analysis of this derivation brings out several important characteristics of the constants K_1 and K_2; but first, a more formal expression of the Rohrer equation should be given. Since air flow may be positive or negative and ΔP must always reflect that sign, Equation 14 should be expressed

(15) $$\Delta P = K_1\dot{V} = K_2|\dot{V}|\dot{V} \ .$$

Airway resistance now becomes

(16) $$R = K_1 + K_2|\dot{V}| \ .$$

From the analysis performed by Collins[42], K_1 is resistance due to laminar flow and is proportional to gas viscosity and independent

of density, and $K_2|\dot{V}|$ is resistance due to turbulent flow and K_2 is proportional to gas density and independent of viscosity.

Though the Rohrer equation is often cited, it is seldom used. Investigators, in general, defer to the laminar flow equation (Equaion 13) and assume R to be constant for the sake of simplicity. Clinical convention would have resistance recorded when flow is near 0.5 liter/sec though this is not rigidly adhered to and most often flow rate is not mentioned when resistance data is presented.

Fry and Hyatt[6] have developed a model to study the mechanics of airway resistance which involves a much deeper analysis than Rohrer's. Their model, though consisting of only a single lung chamber and airpassage, is an excellent example of how simple models may be used to examine and explain complicated biological processes. Their model (see Figure 8) emphasizes the elastic character of the airpassages. They divided the conductive zone into two regions: those interior (region I in Figure 8) and those exterior (region E) to the lungs proper. During expiration the airways exterior to the lung tissue will be subject to high pleural pressures on the outside and low pressures, due to the pressure drop down the airpassage, on the inside. This inward directed transmural pressure gradient will cause constriction of the airpassage. Since, by Poiseuille's Law, resistance is inversely proportional to the fourth power of the radius, a small reduction in cross-section of the tube may increase resistance dramatically. During inspiration the opposite process may be noticed.

In region I the transmural pressures may not be as great as those in region E as region I is subject to lung pressure rather
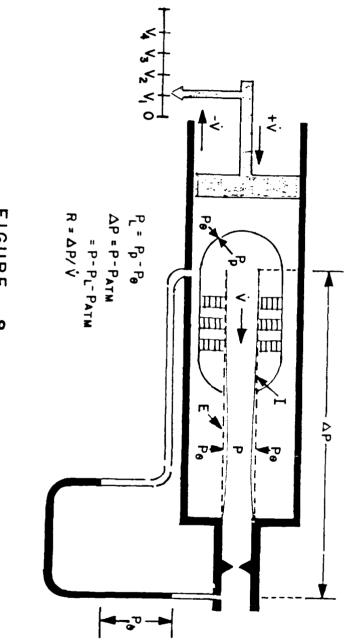
FIGURE 8

$P_L = P_p - P_\theta$

$\Delta P = P - P_{ATM}$

$= P - P_L - P_{ATM}$

$R = \Delta P / \dot{V}$

than pleural pressure; but, the airpassages in this region are, in general, more compliant. Things are further complicated as these airways are supported by surrounding lung tissue such that their diameters will be affected, not only by their own elastance, but also by pulmonary elastance, hence, lung volume.
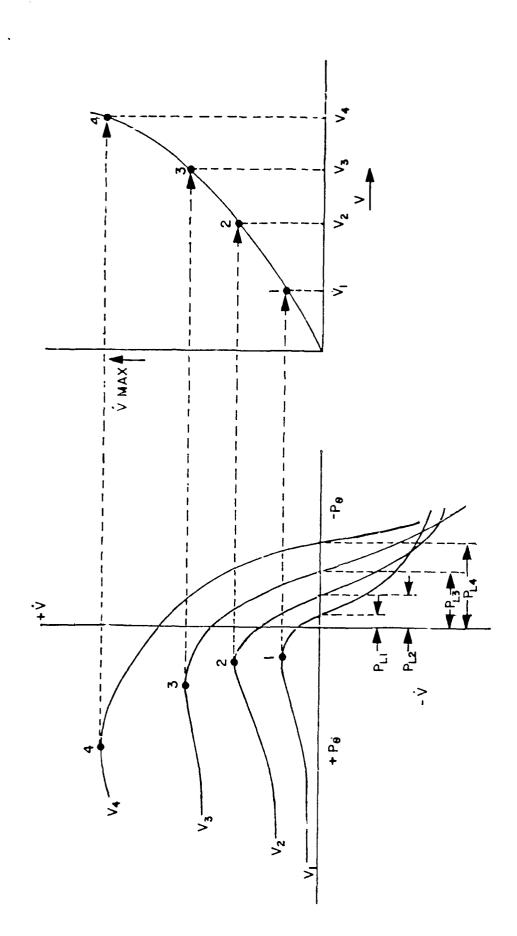
Results from the Fry-Hyatt model indicate that for a given lung volume a driving pressure should exist which yields a maximum flow rate (Figure 9). If the driving pressure is further increased, flow rate will either plateau or decrease due to airway collapse. These results were born out nicely when they made measurements on human subjects (see Figure 10). This indicates that it is not enough to specify the flow rate at which a resistance is given; the lung volume must likewise be specified.

While Fry and Hyatt's model points out some important and interesting aspects of airway resistance, it is not easy to apply them to Rohrer's resistance equation and they made no mention of it. The Rohrer constants, constants K_1 K_2 in Equations (15) and (16) cannot be experimentally separated such that data describing either independent of the other may be obtained. As an attempt at incorporating Fry and Hyatt's results into the Rohrer formalism, this author used the following equations:

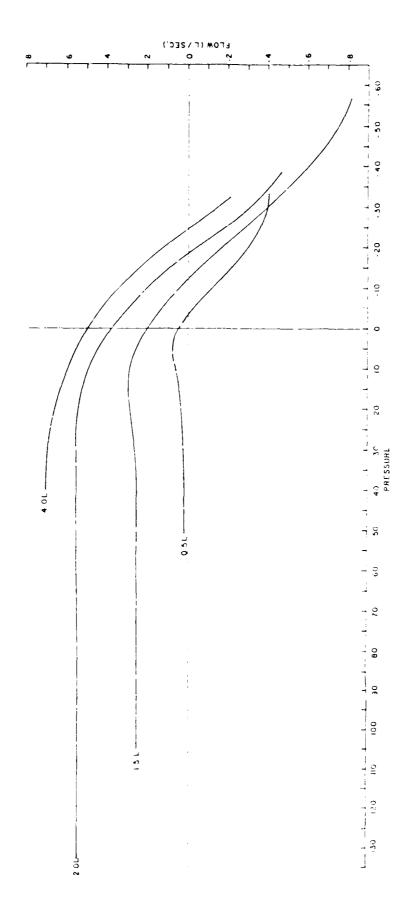$$(17) \qquad K_1 = \frac{B_1 + B_2 P}{1 + B_3 V}$$

and

$$(18) \qquad K_2 = \frac{B_4 + B_5 P' + \frac{1}{2} B_6 (2P_{pl} - P)}{1 + B_7 V}$$

PRESSURE, VOLUME, FLOW RELATIONSHIP

FIGURE   9

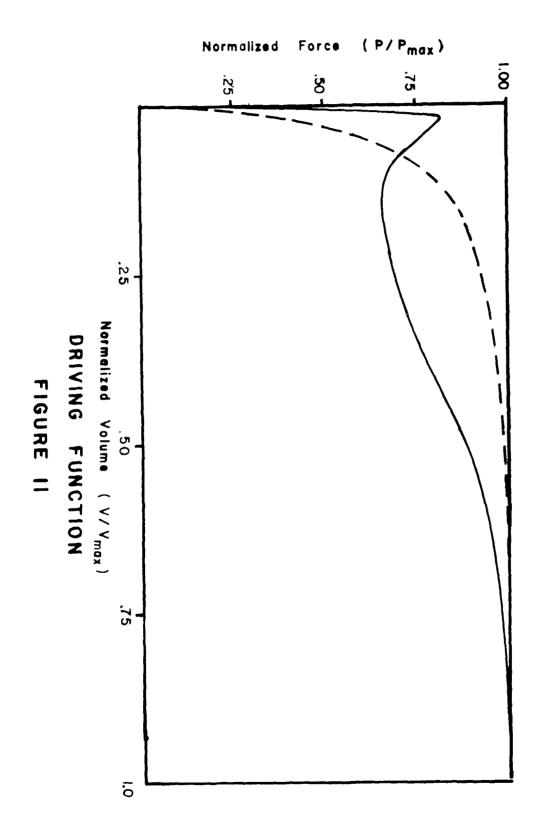ISO-VOLUME PRESSURE FLOW CURVES

FIGURE 10

where $B_1 - B_7$ are constants and P' is the transmural pressure.
These equations allow for an increase in resistance due to
increased transmural pressure or decreased lung volume. The
constants $B_1 - B_7$ were set experimentally by running the model
and comparing the predicted flow-volume curves obtained with those
observed clinically.

For moderate flow rates this set of equations performed
adequately; for the high flow rates observed in the maximum
expiratory flow-volume (MEFV) test, however, it soon became
apparent that no amount of adjusting of the constants $B_1 - B_7$
would yield the desired curve. This problem was partially remedied
by modifying the shape of the driving function from that of a
simple exponential rise to an asymptote represented by the dashed
line in Figure (11) to a function yielding the torturous curve
represented by the solid line. The shape of this final curve was
justified as follows:

a) a rapid isometric rise in pressure to near maximal,

b) a drop in pressure as inertia is overcome, and

c) a slow isotonic rise to maximum pressure.

This was disappointing as it indicated that inertial effects of the
muscle mass which were assumed small in developing the equations
of force balance were indeed significant and would have to be
incorporated into the driving function for every breathing maneuver
examined.

While attempting to model emphysema several problems surfaced
which caused serious doubt as to the validity of the resistance and
compliance equations. To model a mild case of pulmonary emphysema

Normalized Force (P/P$_{max}$)

Normalized Volume (V/V$_{max}$)
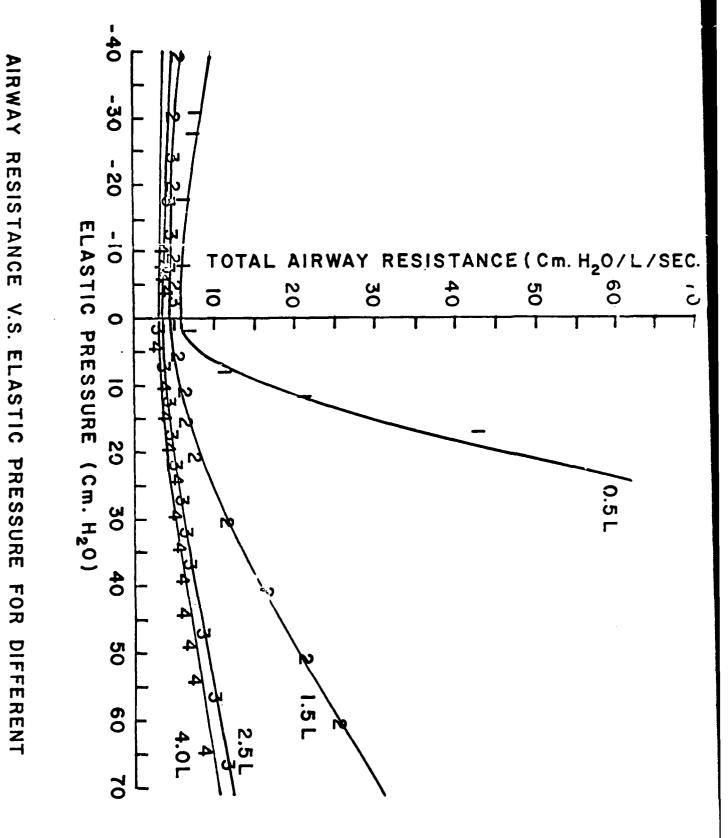
DRIVING FUNCTION

FIGURE II

in the absence of interstitial fibrosis it should only be necessary to lower the compliance of the affected area. When this was attempted, however, the resulting FEFV curves did not display shapes characteristic of emphysema and no amount of adjusting of the compliance curves or the forcing function seemed to help. This forced a reevaluation of both the compliance curves, as will be discussed in the next chapter, and the Rohrer resistance equations.

At this point, it was decided that rather than trying to pick new equations "out of hat" to replace Equations (17) and (18), and adjust them to match flow-volume-pressure data with no guarantee of success, it would be better to work backwards from the observed data and develope an equation which adequately described resistance. This unfortunately meant the Rohrer resistance equation had to be abandoned in favor of a curve fit. The only real loss entailed by this change is in flexibility, as the effects of altering gas density and viscosity cannot be studied as readily. This is only a minor concession, however.

Fry's data (Figure 10) is given in three dimensional form with coordinates of flow, volume, and transmural pressure. This can be converted to resistance, volume, pressure data using Equation (13) where

(19) $$P = P_{pl} - P_{el_{st}}$$

where P_{pl} is the transmural pressure and $P_{el_{st}}$ is the static elastic pressure, i.e., the pressure at the point of zero flow for a given volume. When this transformation was performed and the data plotted the family of curves shown in Figure (12) was obtained.

AIRWAY RESISTANCE V.S. ELASTIC PRESSURE FOR DIFFERENT
VOLUMES ABOVE R.V.

FIGURE 12

The left and right side of each curve may be described as the
left and right sides of a pair of hyperbolas that share a common
major axis on the resistance axis, a common center and focal point,
but have different asymptotes. The two sides, representing
inspiration and expiration, of each curve were fit to the hyper-
bolic function

(20) $$R = B + M[-C + (C^2 + P^2)^{1/2}]$$

where B is the resistance at zero flow, C is half the minor
axis, and M is the slope of the asymptote, each of which may be
approximated graphically.

Once a set of values for the parameters B, C, and M describing
each curve were obtained the volume dependence of each could be
modeled by a curve fit. The following equations were chosen:
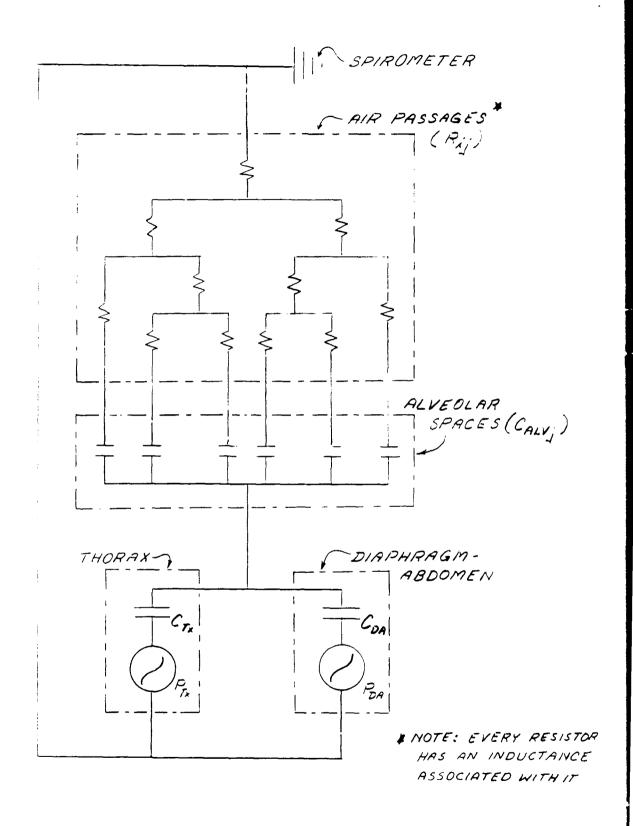
(21) $$B = 6.472 - 1.665 \ V + .2088 \ V^2$$

(22) $$C = 30.0$$

(23) $$M_{insp} = 0.0974/V$$

(24) $$M_{exp} = \frac{.974}{V^{1.48}} \left(1 + \frac{0.25}{V^{2.5}}\right)$$

An electrical analog (Figure 13) was employed in the
distribution of these parameters to the individual air passages
such that when summed, the resistance predicted by Equations (20-24)
was obtained. This was accomplished by making a series of simplifying
assumptions. As a first approximation the lungs were assumed to be
symmetric; thus, Figure (13) simplifies to the analogue depicted in

SPIROMETER

AIR PASSAGES *
(R_{A_j})

ALVEOLAR
SPACES (C_{ALV_j})

THORAX

DIAPHRAGM-
ABDOMEN

C_{Tx}

C_{DA}

P_{Tx}

P_{DA}

* NOTE: EVERY RESISTOR
HAS AN INDUCTANCE
ASSOCIATED WITH IT

ELECTRICAL ANALOG

FIGURE 13

Figure (14-A) where the subscripts R and L indicate the right and left sides of the lung and R_R is equal to R_L. The total resistance of the system is

$$(25) \qquad R = R_2 + \frac{R_L R_R}{R_L + R_R} = R_2 + \frac{R_L^2}{2R_L} = R_2 + \frac{1}{2} R_L \ .$$

Substituting Equation (20) into Equation (25) with appropriate subscripts yields

$$(26) \qquad B + M[(C^2 + P^2)^{1/2} - C] =$$

$$B_2 + M_2[(C_2^2 + P_2^2)^{1/2} - C_2] + \frac{1}{2} \{ B_L + M_L[(C_L^2 + P_L^2)^{1/2} - C_L] \} .$$

Since P on the left of the equation is the pressure drop throughout the system,

$$(27) \qquad P = P_2 + P_L \ .$$

The constant C has units of pressure and it was assumed that when P equals C, it would follow that P_L would equal C_L and P_2 would equal C_2 such that

$$(28) \qquad C = C_2 + C_L \ .$$

Further examining Equation (26), we find that when P equals zero,

$$(29) \qquad B = B_2 + \frac{1}{2} B_L$$

and if P is equal to C,

$$(30) \qquad M = \frac{2}{C_L} (MC - M_2 C_2) \ .$$

Employment of Equations (28-30) assures that whatever values are assigned to the distributed constants in Equations (21-24), for the
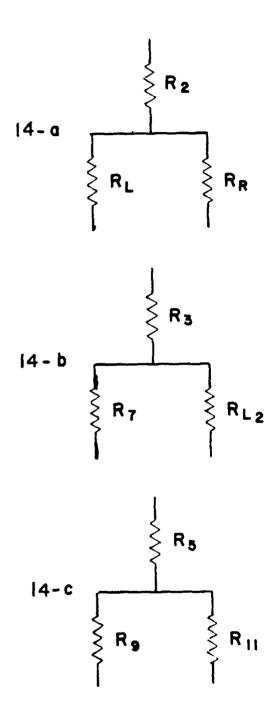
FIGURE   14

resistance R_2, the total resultant resistance will be approximately that predicted by Equation (20).

The equations describing the distribution of resistance parameters to the lower regions were developed in a similar manner using the resistance analogs depicted in Figures (14-B) and (14-C) and will not herein be detailed. It is, however, important to list the assumptions made.

1) As R_2 represents resistance to flow through air passages exterior to the lung, it should not be a function of lung volume.

2) The dependence of resistance on volume increases as one descends into the lung due to the disappearance of the supporting rings of hyaline cartilage.

3) In the supine position, when the gravitational pressure gradient disappears, the total pressure drop to each alveolar chamber should be the same.

The results of this curve fit are illustrated in Figure (12), where the digits indicate original data[6] and the solid lines are the curve fits. The effects of the changes in the handling of airway resistance on the dynamics of the system, especially the forcing function, shall be discussed at the close of the following chapter on compliance.

IV. COMPLIANCE

For clinical purposes, compliance is defined in terms of a single chambered lung model in which a spring represents elastance.[7] For such a model, Hook's law states that elastic pressure will be proportional to the volume displacement from the equilibrium volume, V_r, which is the volume the lung would assume if elastance were the only force acting on it; thus,

$$(31) \qquad P_{el_L} = \frac{1}{C_L} (V_L - V_E) \ .$$

The equation describing the balance of forces across the alveolar wall in such a model is just Equation (6) here repeated as

$$(32) \qquad P_{alv} = P_{pl} + P_{el}$$

where the hydrostatic pressure is included in P_{pl}. The equation describing flow is Equation (13);

$$(33) \qquad P_{alv} - P_{mo} = R_T \dot{V}$$

where P_{mo} is pressure at the mouth, R_T is total air resistance, $\dot{V}$ is volume flow rate, and inertance is assumed negligible. Combining these three equations yields

$$(34) \qquad P_{mo} - P_{pl} + R_T V = \frac{1}{C_L} (V - V_E) \ .$$

Due to problems in determining R_T, compliance is always determined at instants of no flow where Equation (34) simplifies to

$$(35) \qquad P_{mo} - P_{pl} = \frac{1}{C_L} (V - V_E) \ .$$

Since $\dot{V}_E$ cannot be measured indirectly, zero flow must be established for at least two different lung volumes, such that C_L may be determined through Equation (35) as
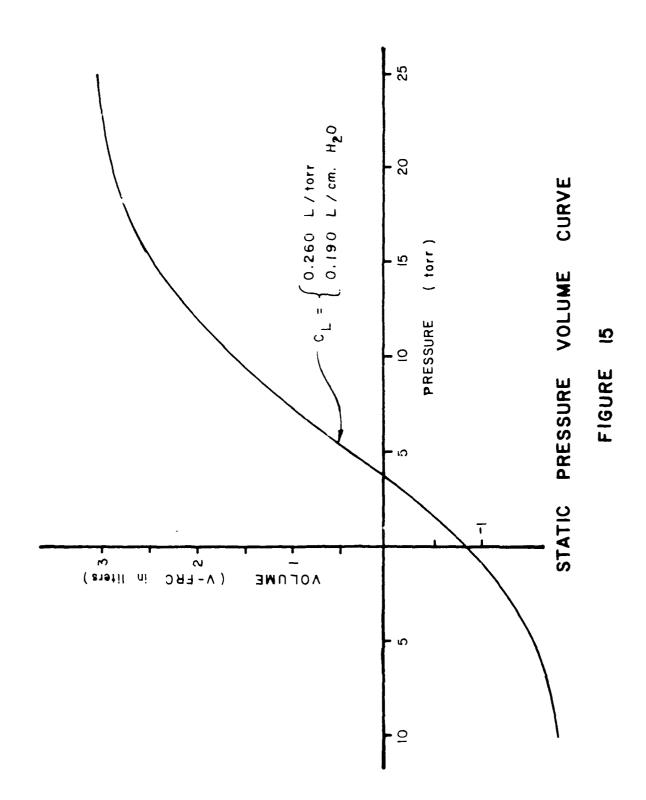
$$(36) \qquad\qquad C_L = \frac{-\Delta V}{\Delta P_{pl}}$$

where C_L is assumed constant over the volume range, ΔV. This equation is just the difference form of the common definition of compliance which is

$$(37) \qquad\qquad E = \frac{1}{C} = \frac{\partial P_{el}}{\partial V} \, ,$$

where E is elastance.

The clinical procedure for measuring C_L using Equation (36) is to have the subject inspire a small volume of air and hold it until equilibrium is reached throughout the lungs. The pleural pressure is measured before and after the process with an esophageal balloon (a slender, very compliant balloon inserted through the nasal passages, past the epiglotis, and positioned midway down the esophagus which may be inflated to a known pressure and used to monitor changes in pressure in the thoracic cavity) and V_L is measured with a spirometer. This, after a number of such measurements, yields the static pressure-volume curve; the slope of which is "static" compliance. Figure (15)[43] illustrates such a curve.

The static compliance curve indicates clearly defined lung volume maxima or total lung capacities (TLC) of between 5.5 and 7.0 liters, depending on the subject's height and age, with 6.0 liters being the norm. This is curiously lower than results obtained from excised

$$C_L = \left\{ \begin{array}{l} 0.260 \ L/torr \\ 0.190 \ L/cm. \ H_2O \end{array} \right.$$

PRESSURE (torr)

VOLUME (V-FRC in liters)

STATIC PRESSURE VOLUME CURVE

FIGURE 15

lungs by many investigators as reviewed by Hoppin and Hildebrandt[44] who quote figures of 12 to 14 ml gas per gram lung weight. The average lung weighs approximately 1.2 kg[45] which yields an expected TLC of 14 to 17 liters, more than twice that observed clinically. A reasonable explanation for this difference in measured TLC has not been found.

During the early stages of development of the model the compliance curve described by the excised lung experiment was selected over the invivo clinical measurement. It seemed the more direct procedure and the use of the esophageal balloon to approximate pleural pressure is subject to criticism as it includes the compliance of the esophageal wall. Furthermore, it would seem that lung tissue, being more delicate than the muscles and bone surrounding it, should not furnish the elastic limits of the system.

The equation chosen by this author to model the static compliance as depicted in Figure (15) is

$$(38) \qquad P_{ei} = \frac{A}{A_1 * \frac{1}{2}} \tan \left[\frac{(V - A_2)}{2A} \right] + A_5$$

where

$$(39) \qquad A = A_2 - A_4$$

when the volume V is less than A_2 and

$$(40) \qquad A = A_3 - A_2$$

for V greater than A_2; A_1 is the slope at the point of inflection, A_2 is the volume at the point of inflection, A_3 is the lower asymptote, A_4 is the upper asymptote, and A_5 is the pressure at

the point of inflection. The compliance constants were then
distributed to the various pulmonary elements in a manner analogous
to that described in the last chapter for resistances. All lung
tissue chambers are assumed to be identical as there has been no
evidence indicating different characteristics of tissue from different
regions of the lung. This allows that in the supine position, where
the hydrostatic pressures are equal, all lung chambers are of equal
volume.

As stated in the previous chapter, problems arose when a purely
compliance oriented disease, emphysema, was examined which necessitated
the reevaluation of the compliance philosophy. This was accomplished
by developing and examining a simple model of how the esophageal
balloon measures pleural pressure (See Figure 16). Both pleural and
esophageal chambers are assumed to be filled with incompressible fluid
and the balloon is filled with compressible gas. The force balance
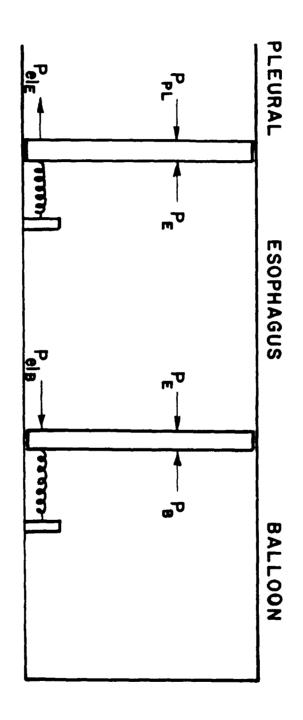equations for the two pistons are

(41)
$$P_{pl} = P_{el_E} + P_E$$

and

(42)
$$P_B = P_E + P_{el_B} .$$

Combining Equations (41) and (42) yields

(43)
$$P_{pl} - P_B = P_{el_E} - P_{el_B} .$$

Assuming P_{el_B} is to be negligibly small, a good assumption considering
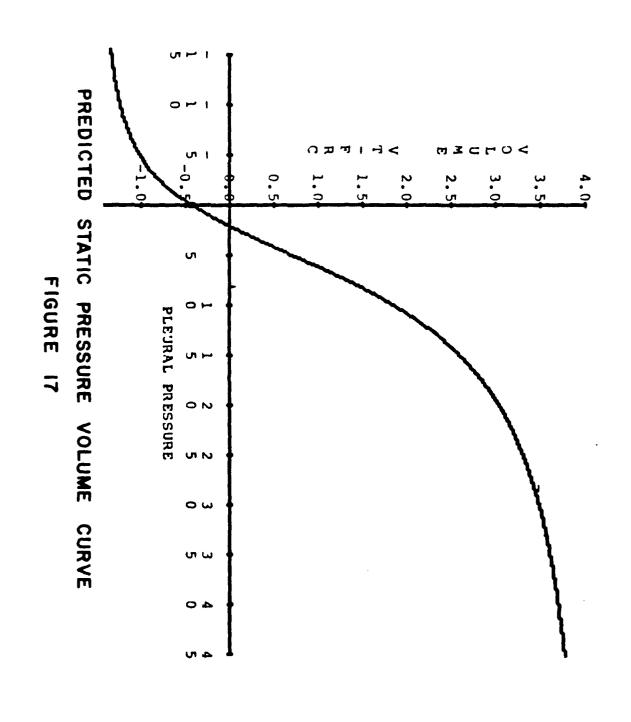the compliance of the balloon used, and rearranging Equation (43) yields

ESOPHAGEAL BALLOON MODEL

FIGURE 16

(44) $$P_B = P_{pl} - P_{el_E} \ .$$

Since the balloon is inflated slightly, P_{el} will be negative in the direction of the arrow in the figure. This implies that the observed balloon pressure cannot be less than the pleural pressure and, therefore, the esophageal elastance cannot be used to explain the disparge between in-vivo and excised lung data. Furthermore, since the upper volume limit of the lung cannot be less than that indicated by the balloon pressure curve, it was determined that esophageal compliance must be relatively large such that P_{el_E} contributes little to P_B. P_B should, therefore, provide a good approximation of the pleural pressure.

This discovery dictated the abandonment of excised lung compliance curves in favor of in-vivo curves. Figure (17) gives the new compliance curve generated by the model which should be compared to the compliance curve for a human subject (See Figure 15).
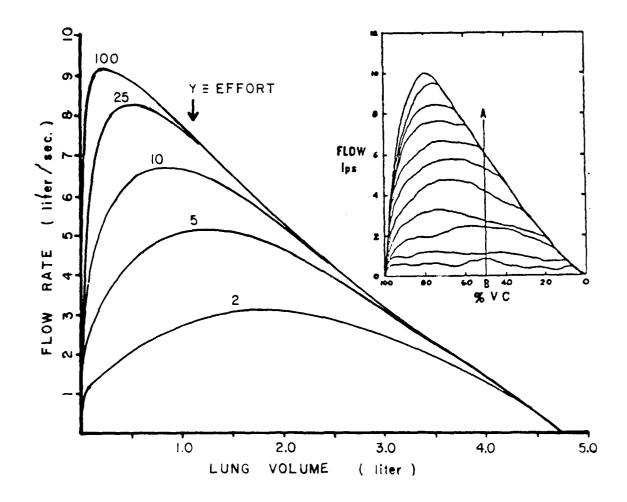
The initiation of the modifications, herein descirbed in the compliance equations and the changes in the resistance equations discussed in the previous chapter caused one unforseen problem; the modified Newton-Raphson method of solving the steady state pressure equations in the airways failed to converge under certain conditions and had to be abandoned. A numerical method was developed whereby the pressure dependence of the airway resistance is neglected during a single iteration. This allows the new pressure to be calculated from the mass-balance equations linearly. Resistance is then calculated in terms of the new pressures and the process is repeated. This iteration scheme solved the problem and proved more stable than the modified Newton-Raphson method.

PREDICTED STATIC PRESSURE VOLUME CURVE

FIGURE 17

The solution of this series of problems proved to be a major advance in the continued development of the model. Not only did it allow the examination of lung mechanics in the most nonlinear operational regions, but it cleared up several problem parameter areas that had nagged at the credibility of the model since the first runs. As has been mentioned, the predicted static compliance curve now provides a much better match to clinical data. A second improvement is in the formulation of the driving function representing contraction of the respiratory muscles.

As was discussed in the previous chapter, the examination of forced expiratory breathing maneuvers has been hampered by the sensitivity of the FEFV curve to the form of the driving functions. With the incorporation of the new resistance and compliance changes this problem disappeared. What had appeared to be a necessity to incorporate inertial effects of the muscle masses into the driving functions proved to have been problems with the resistance and compliance equations that could be partially compensated for by altering the form of the driving function.

Good correlation between model predictions and clinical results for a number of forced breathing maneuvers has now been obtained, this using only the simple exponential form for the driving function as used for passive breathing maneuvers, Equation (12) with appropriate values for the constants. Figure (18) illustrates the results of several simulations of forced expiratory breathing maneuvers using different values for the constant y. This is precisely like the family of curves reported first by Fry and Hyatt[46] for a series of graded effort FEFV maneuvers (See inset on Figure 18).

VARIABLE EFFORT FLOW VOLUME CURVES

FIGURE 18

This study determines values for two important lung parameters which need setting prior to the WBA studies. These are the maximum P_x that may be generated by muscular contraction and the maximum rate of muscular contraction, i.e., P_{max} and the maximum value for y. P_{max} is now set at 118 mm Hg and the maximum value for y is set at 75.

V. Whole Body Acceleration

As stated in Chapter I, the effects of WBA on the human pulmonary system are difficult to ascertain using traditional techniques due to difficulties in collected data on human subjects and due to the inadequacy of animal models. It is proposed that the mathematical simulator of the human pulmonary system already described, if supported by a limited amount of data to verify the model's preductions, may be used to remedy deficiencies in existing data and explain observed, but poorly understood, phenomena in terms of overall lung dynamics as well as regional parameters heretofore inaccessible. In this chapter we will attempt to use the model to establish a basic understanding of pulmonary mechanics and to evaluate a technique employed to reduce the adverse effects of WBA and improve G-tolerance, that of altering the angle of attack of the G-forces.

It has long been recognized that at some seat tilts pilots are able to withstand greater WBA than at others. U.S. Air Force studies have considered angles of 23°, 28° and 40° as the seatback angles for the F-15, YF-16, and YF-17 fighter planes. Results reported by Gell[47] indicate that seat tilts of less than 45° do not yield significant improvement in WBA tolerance and both Crossley[48] and Burns[49] report that for seatback angles of 65° to 75° tolerance improves sharply. These reports are for the most part based on subjective observations of pilots and, therefore, provide only very loosely defined ranges of optimal seatback angles.

In the attempt to gain a better understanding of the operation of pulmonary mechanics under WBA and how changes in the vector direction of the applied G-forces alter those mechanics, several lung parameters that have long been recognized as being of importance clinically will be examined. Lung mechanics may be broken down into two broad headings: 1) Statics and 2) Dynamics. Under the topic of statics, we shall examine changes in

A)   Functional Residual Capacity and

B)   regional distribution of resting volume.

Under the topic of dynamics, we shall concentrate on

C)   Dynamic Compliance Loops and

D)   the work of breathing.
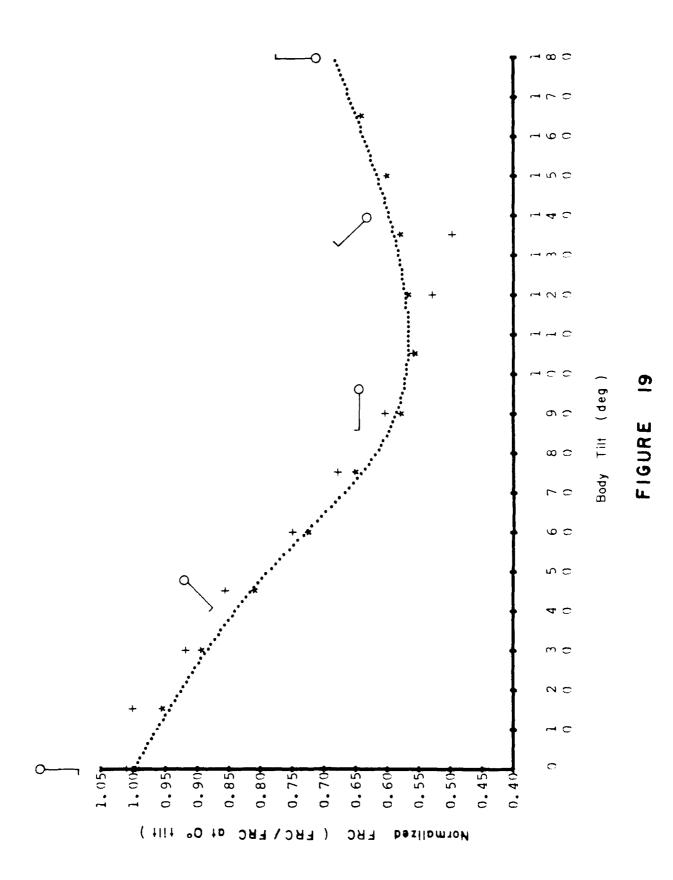
Study A: Functional Residual Capacity

In the study of the combined effects of WBA and seatback angle on lung parameters, the first area to be examined will be that of Functional Residual Capacity (FRC). This is the equilibrium volume of the lung where all respiratory muscles are in their relaxed state, i.e., the volume of the lung at the end of relaxed expiration from which active inspiration starts. Consequently, FRC defines that region of the compliance curve over which the lung operates during normal breathing. Since normal FRC in the erect position falls near the most compliant portion of the static volume-pressure curve, it would seem that maintainance of near normal FRC would prove most conducive to WBA tolerance.

The effect of change in body tile with respect to earth normal gravity was once an area of intense medical interest, consequently, much data is available. In the 1920's and 30's, it was well known that changing a subject from an upright to a prone position while lying in a bed caused a reduction in FRC of one to one and a half liters. The data presented as plus "+" symbols in Figure (19) are taken from a more recent source, Agustoni,[50] but are exemplary of the type of data presented by early researchers and illustrate observed changes in normalized FRC when tilting a subject from an upright position, 0° tilt, to 135° head down tilt. Early workers capitalized on this and used a tilting bed to respirate subjects with paralized respiratory muscles. Fortunately, the iron lung was invented and this technique was abandoned.

The dotted line in Figure (19) illustrates the results of using the model to simulate the change in FRC brought about by body tilt. Clearly, for the first 90° to 100° moderately good correspondence with the literature data is achieved. Beyond 100° tilt the model predicts that FRC will increase while the clinical data continues to drop.

Agostini,[50] however, demonstrated that FRC measurement is dependent on the method of restraint used during the position changes. He points out that the "+" symbols are characteristic of data collected when the subject is supported by the shoulders and the asterisks "*" are characteristic of data collected when

Body Tilt (deg)

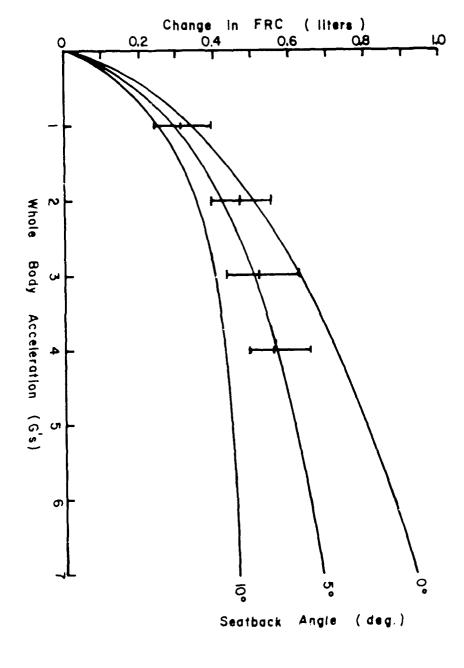Normalized FRC (FRC/FRC at 0° tilt)

FIGURE 19

supporting the subject by the ankles. The reasons for the model's

acting as if it were supported by the ankles are not known at

this time, though, it must be a characteristic of the geometry of

the components chosen. As we are not, at this time, concerned

with bed ridden subjects this is a plus rather than a detriment.

Glaister[51] reports how FRC responds to changes in $+G_z$

acceleration. His data, including error bars, are reproduced in

Figure (20). Glaister did not, however, describe the details of

how the subject was mounted in the centrifuge. It may be assumed

that he had the subject seated in a standard pilot's seat with

the back in an upright position. The back of a pilot's seat, as

with any other seat, is not exactly vertical, but is set at some

small angle. The results of three attempts to simulate Glaister's

results using different seatback angles (0° true vertical, 5°,

and 10°) are presented as solid lines in Figure (20). If these

assumptions are valid, the simulated data match Glaister's results

nicely.

If the model has the capability of predicting changes in

FRC with respect to changes purely in body angle and with respect

to changes purely in WBA, the model provides a valid tool for

the examination of the combined effects of seatback angle and WBA

on FRC. Figure (21) is a three dimensional representation of such

a study where seat tilts of 0° to 90° and WBA of from 1 G

earth normal to 10 G's are examined. The 1 G iso-gravity curve

is the same as that presented in Figure (19) and the 0° to 10°

iso-angle curves are the corresponding curves from Figure (20).

Change in FRC (liters)

Whole Body Acceleration (G's)

Seatback Angle (deg.)

10° 5° 0°

Data points with error bars are averages obtained during positive acceleration. (Glaster)
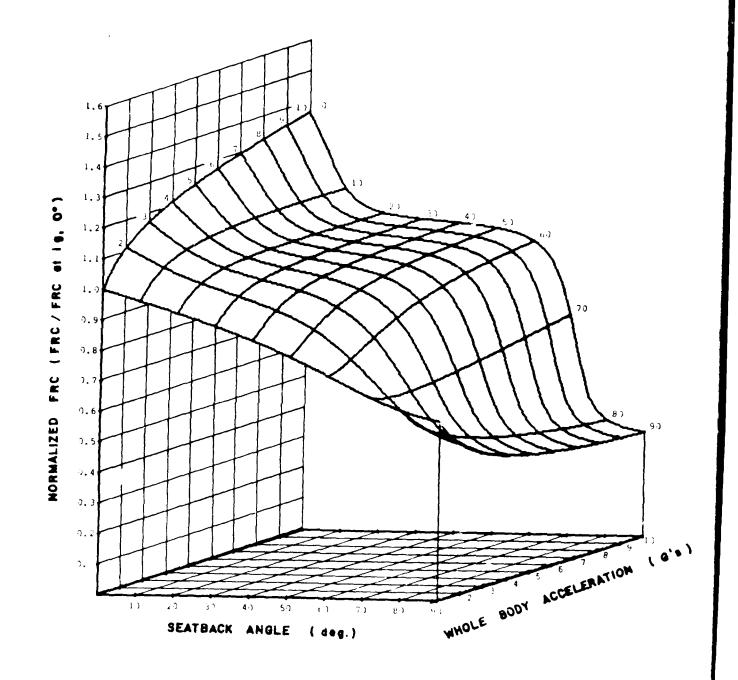Solid lines are model predictions.

FIGURE 20
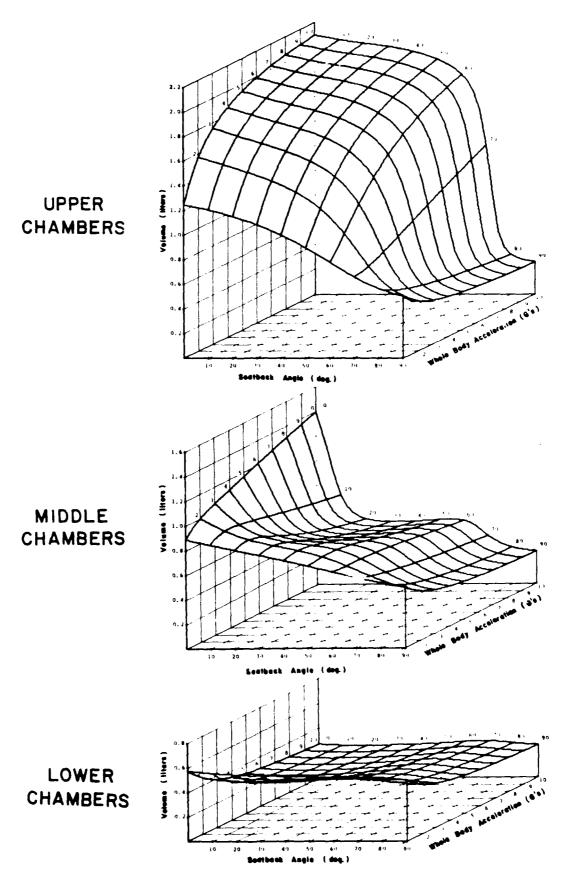
FIGURE   21

If we accept our earlier hypothesis that maintaining near normal FRC while undergoing high sustained WBA is ideal, this' study indicates that any seatback angle from 15° to 65° is acceptable. Figure (21), however, provides only gross lung data and before a "best angle" is chosen, the behavior of individual chambers should be examined.

Study B: Regional Distribution of Resting Volume

Figure (22) is a breakdown of the data from Figure (21) into regional values. Each region has a maximum volume of 2.28 liters and a minimum volume of 0.22 liters. It may be noted that for 1 G and 0° tilt, the upper chambers have more than twice the volume of the lower chambers. This is a reflection of the increase in hydrostatic pressure in the pleural fluid caused by the 1 G_z force as was first measured by Glazier[31] (see page 15). Glazier further demonstrated that when G_z was increased, this effect was magnified. This fact corroborates the models results when the 0° iso-angle curves for each region are compared.

Examining the predictions for the lower chambers, we find that increased WBA has caused a reduction in regional volume to near the minimum volume. This would place this region on the lower end of the pressure-volume curve where it would be very noncompliant. Changes in seatback angle do not have appreciable effect in this region. The upper chambers behave much differently in that for low seat tilts, increase in WBA causes the volume to

UPPER
CHAMBERS

MIDDLE
CHAMBERS

LOWER
CHAMBERS

LOCAL FRC IN THREE LUNG REGIONS

FIGURE 22

approach its maximal value. This trend is not appreciably affected until seatback angle reaches a very narrow range of between 60° and 70° where FRC begins to plunge toward its lower limit. At angles of 80° to 90°, the upper chamber is also near its minimum volume. The middle chambers offer the most interesting study in that there are two possible optimum angles: 10° and 60°.

In summation, the gross lung FRC data presented in Figure (21) do not provide the detail necessary to determine an optimum seatback angle. It does, however, provide results which may be used to confirm the ability of the model to simulate static lung mechanics. An examination of regional FRC provides two angles as possible candidates for consideration as optimum seatback angles, 10° and 60° to 70°, i.e.,

i) if, due to other considerations, it seems advisable to force the best ventilation to occur in the middle chambers, this may be accomplished by choosing an angle near 10°, or

ii) if it be deemed advisable to share the best ventilation between all of the chambers, then an angle of between 60° and 75° should be considered.

A choice between these alternatives cannot be made on the basis of a single study but will be reconsidered in the next chapter when more information is available.
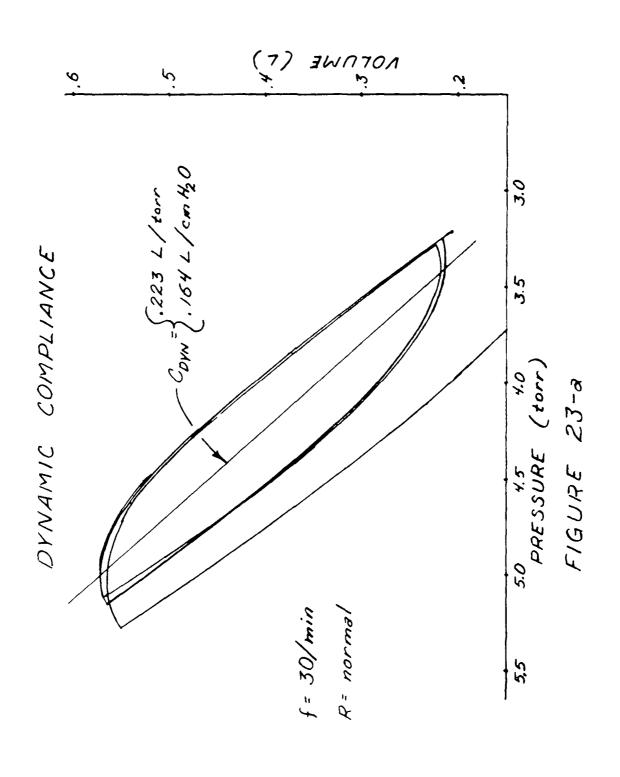
Study C: Dynamic Compliance
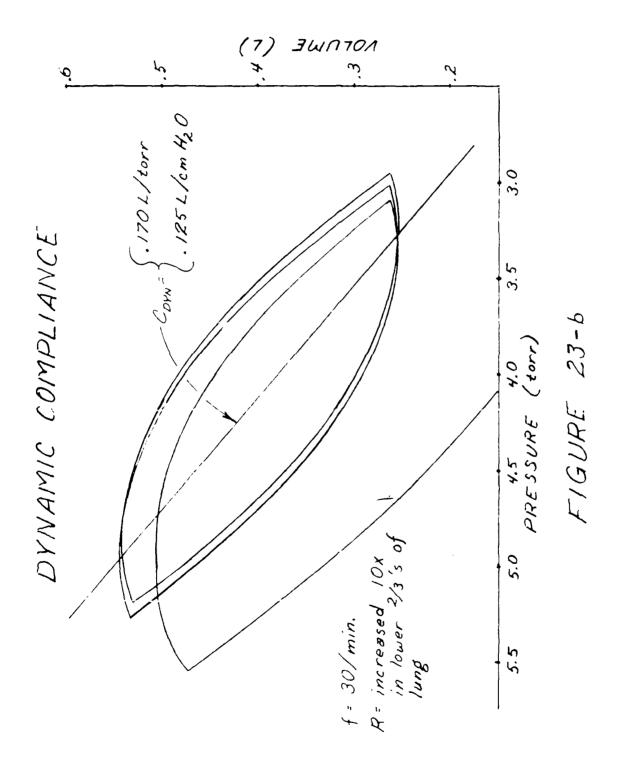
In Chapter IV the concept of static lung compliance is developed and the measurement technique is discussed. As was therein mentioned, compliance is determined at instants of zero flow such that resistance is eliminated from the measurement. A second technique for approximating the compliance utilizes the instant of zero flow at the mouth that occurs naturally at the beginning and end of inspiration. This procedure, which determines the "dynamic compliance," calls for the subject to breath small tidal volumes around FRC, such that compliance should change little throughout the breath. The procedure may, however, be criticized as the value obtained is not pure compliance. The fact that flow has ceased at the mouth is no indication that flow has ceased throughout the lungs. Since lung volume and pleural pressure are out of phase with each other and since dynamic compliance is determined during a dynamics rather than a static state, flow will be occurring in the peripheral airways (those nearest the acini) and Equation (34) rather than (35) should be employed to determine C_L.

Though this criticism indicates that the value determined for C_{Dyn} is not a compliance in the true sense, it leaves us with some interesting consequences. Flow is occurring and dynamic compliance will, therefore, be a function of the resistance and the flow rate. Since the procedure dictates that flow in the upper airways be near zero, a change in C_{Dyn} must be a function

of peripheral airway resistance only. Peripheral airway resistance
must change drastically before the total resistance is significantly
affected, but, by comparing dynamic compliance to values accepted
as normal, abnormal peripheral airway resistance may be detected
in diseases, qualitatively, far earlier, thus giving advance
warning of the onset of diseases such as asthma and chronic
bronchitis which seem to attack primarily small airways. The use
of dynamic compliance in determining peripheral airway resistance
is further refined by the recognition that the phase shift between
V_L and P_{pl} increases with the frequency of breathing. This
means that the flow in the small airways will increase and
dynamic compliance will better reflect abnormal resistances in
these regions.

Figure (23-a) illustrates the results of a three breath run
starting at FRC in which the resistance was normal and breathing
frequency was 30 BPM (breaths per minute). Figure (23-b) shows
a similar run in which the linear resistance in the lower order
bronchi feeding the lower two thirds of the lung was increased
tenfold. The drop in compliance and the widening of the P-V
loop expected clinically as a result of high small airway
resistance is evident. The increase in total resistance associated
with this large increase in lower order resistance was only by a
factor of two, however, and remained within the normal range.
Such an abnormality might go unnoticed if further tests were not
run on the subject. A study of frequency dependence of C_{Dyn}

DYNAMIC COMPLIANCE

$C_{DYN} = \begin{cases} .223 \ L/torr \\ .164 \ L/cm \ H_2O \end{cases}$

VOLUME (L)

PRESSURE (torr)

FIGURE 23-a

$f = 30/min$

$R = normal$

DYNAMIC COMPLIANCE

$C_{DYN} = \begin{cases} .170 \text{ L/torr} \\ .125 \text{ L/cm } H_2O \end{cases}$

VOLUME (L)

.6
.5
.4
.3
.2

3.0   3.5   4.0   4.5   5.0   5.5
PRESSURE (torr)

f = 30/min.

R = increased 10x
in lower 2/3's of
lung

FIGURE 23-6
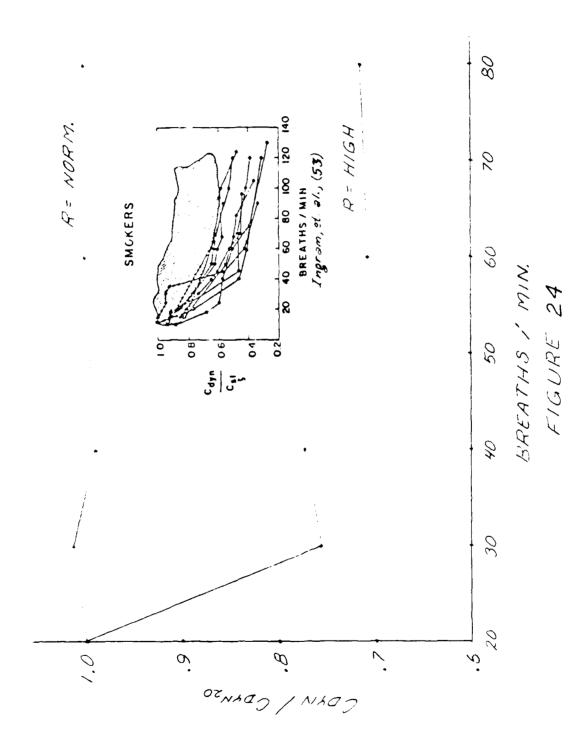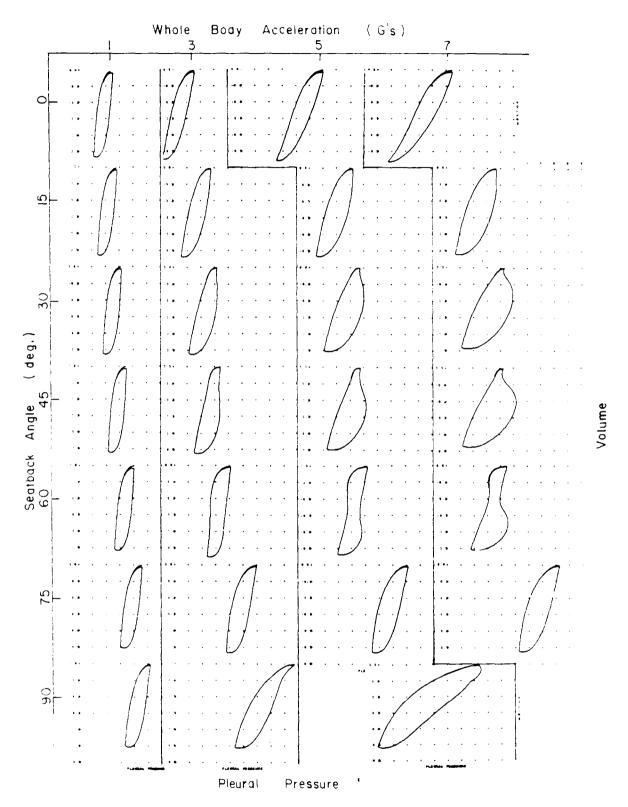
performed on the same subject, provided in Figure (24), more clearly
indicates the problem. The shape of the high resistance curve
very nicely matches the experimental results observed by Ingram,
et.al.[53], in their study of apparently healthy smokers which are
included as an inset to Figure (24). The shaded area in the
inset is the range in which compliance of the normal non-smokers
fell. (Note: The study using the model only included frequencies
up to 80 BPM and is shifted up with respect to the inset values
due to a different definition of normalization, i.e., $C_{Dyn}/C_{Dyn_{20}}$
rather than C_{Dyn}/C_{st}.)

Due to the difficulty of obtaining dynamic compliance loops
for subjects undergoing WBA, no information has been published
indicating how WBA affects dynamic compliance. If, however, we
accept that the model is adequately simulating system dynamics
under earth normal gravity as indicated by the above mentioned
dynamic compliance studies, the passive breathing study (Chapter II),
and the variable effort forced maximal expiration study (Chapter IV),
and if we accept that system statics are being adequately simulated,
as indicated by the arguments presented in Studies A and B of
this chapter, the model should provide a good simulation of system
dynamics under WBA.

In Figure (25) are given the results of a series of simulated
passive breaths while in different body positions ranging from 0°
(upright) to 90° (supine) and for different levels of WBA ranging
from 1 G to 7 G's. Passive breathing was defined as a two

CDYN / CDYN₂₀

BREATHS / MIN.

FIGURE 24

R = NORM.

R = HIGH

SMOKERS

$\frac{C_{dyn}}{C_{st}}$

BREATHS / MIN

Ingram, et al., (53)

Dynamic Compliance Pressure - Volume Loops

FIGURE 25

second inspiration of about 0.5 liters of air starting at FRC and a 3 second relaxed expiration. Each loop represents a pressure volume plot with each tic mark increasing horizontally representing 2 mm Hg and each tic mark descending vertically representing 0.1 liters of air inspired. (Inspiration is recorded as a negative change in spirometer volume.)

It is interesting to note that, though WBA tends to decrease dynamic compliance, the two angles most affected are 0° and 90° with 90° by far the worse. This result was anticipated from the results of the local FRC study described in Study B of this chapter. The FRC of each chamber is changing and the region is constrained to operate on a different portion of its static compliance curve.

Not only does increased WBA cause an increase in dynamic compliance, it also causes changes in the overall shape of the pressure-volume loop. Shapes such as those suggested for higher WBA and seatback angles of 30° to 60° have neven been observed before. These results should be expected, however, as the lung is no longer operating on the most linear portion of the static compliance curve.

Remembering that the width of the loop is an indication of overall airway resistance we may evaluate this series of runs in terms of both compliance and resistance; the two major characteristics of lung tissue mechanics. Where dynamic compliance is least affected by WBA for tilts of 15° to 75°, resistance appears least affected for tilts of 0° to 15° and 60° to 75°.

The net results of these observations match those obtained by casual visual inspection of Figure (25), i.e., two seatback angles stand out as being optimal for minimizing the effects of WBA on the dynamic compliance angle, the width, and the overall shape of the pressure-volume loops: 15° and 75°.

Study D: Work of Breathing

Since the concern of pulmonary mechanics is the movement of air into and out of the lungs, the mechanical work involved may be expressed as

$$(45) \qquad\qquad W = \int P \, dV \; .$$

To obtain the true work of breathing, P should be the driving pressure generated by the respiratory muscles. This pressure cannot be measured, however, and the pressure difference between pleural pressure and mouth pressure as measured by an esophageal balloon is conventionally used. This would represent the area under the volume-pressure curve of the dynamic compliance loop and would only yield the work performed in overcoming lung tissue elastance and airway resistance, which is of only limited value. The pressures involved in driving the model are known and, consequently, the work of breathing may be calculated as
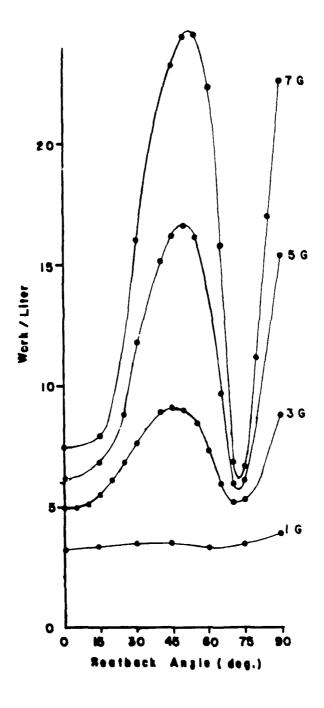
$$(46) \qquad\qquad W = \int P_{Tx} \, dV_{Tx} + \int P_{DA} \, dV_{DA} \; .$$

In general, when biological systems are being examined, it is not mechanical work but expended energy or effort, of which

mechanical work is but a part, which is of interest. Effort,
unfortunately, is both difficult to define and more difficult
to measure in the invivo state. If the entire organism is being
examined, O_2 consumption and heat generation may be used as
indicators. When only certain muscles of the organism are of
interest and especially when that organism is man, who objects
to invasive measurements, expended effort is virtually impossible
to define and mechanical work is often used as an indicator.

Investigators who report the work of breathing often ignore
these facts and a few simple examples may be in order in
clarifying the difference between the two. Were the equilibrium
volume of either the diaphragm or the chest to be forced either
up or down the compliance curve to near the asymptote (see
Figure (15), it would require a tremendous effort to inspire even
a small volume with the muscles of that anatomical element. The
work performed by those muscles would, however, by Equation (46),
be small. If, on the other hand, the system were to be driven
entirely by one muscle complex and the other were to remain passive
and expend no effort, the pressures in the system would cause
movement of the other and Equation (46) would indicate that work has
been performed though no effort had been expended.

Figure (26) gives the results of the calculated work of
inspiration for the simulated breathing studies reported in
Figure (25). Since, for relaxed breathing, expiration is accomplished
by passive relaxation of the respiratory muscles and little effort

Work of Passive Breathing

FIGURE 26

is actually expended, though mechanical work near that of inspiration is performed, only the work of inspiration will be examined. To make comparison to data easier, both muscle groups were constrained to exert equal driving pressures. Work per liter of inspired air is reported as not all breaths were of exactly the same depth. Ignoring the criticisms of using work as a measure of effort cited earlier, it is easy to interpret this family of iso-G curves. Two ranges of seatback angles appear best in minimizing the work of breathing: best is the 70° to 75° range, and surprisingly, of secondary importance is the 0° to 15° range.

Two points are of special interest in examining Figure (26): First, note how independent of seatback angle the work of breathing is in the earth normal 1 G environment. It would seem the system was designed to operate under this condition. Secondly, it is interesting to note how poorly the system responds to WBA in the supine position. This position has been chosen by NASA for the astronauts primarily on the basis of circulatory considerations.

VI. Conclusion

In the preceding chapter we have described four studies of the effects of WBA on pulmonary mechanics using the mathematical simulator developed and justified in the preceding chapters. Each study, to the extent possible, is divided into two parts:

a) verification of simulation results by comparison with existing experimental data and

b) prediction of the effects of WBA on lung mechanics in areas hitherto unexamined.

These will now be discussed in more general terms as they relate to each other.

A. Verification and Criticism of Results:

While the first of these studies, that of the effect of WBA on gross lung FRC, provides the least useful data in terms of defining optimum seat tilt, it is perhaps the most significant as it is the most directly verifiable and provides the best indication that the model is adequately simulating the system. The second study, that of the effects of WBA on local equilibrium volumes, provides a basis for evaluating and understanding other studies. While it is supported by studies involving frozen dogs, it derives its main support from the fact that it contributes the parts from which the previous study involving the gross FRC is compiled.

As we are primarily interested in h· ·v well the lung can function, the last two studies, those in· lving dynamics, must be given the greatest weight. Study C of the last chapter indicates that good correlation between model results and experimental data have been achieved for the earth normal gravity studies; however, due to the difficulties involved, no data are available to corroborate the high WBA studies. Likewise, no data are available to corroborate the work of breathing studies and Study D of the previous chapter discussed many of the pitfalls of using these results in defining difficulty in breathing.

B.   Results

Recognizing the above criticisms of the limitations of the studies thus far carried out, it is, however, necessary to make a final conclusion based upon the data available for selecting an optimum seatback angle for maintaining good respiratory function under WBA.   Summarizing:

Study B indicates a choice between 10°, for which ventilation will be better in the middle chambers, and an angle between 60° and 70° for which ventilation would be more equally distributed.

Study C suggests that angles of 15° and 75° both provide a near normal dynamic compliance loop.

Study D predicts that an angle of near 70° is best, but that an angle of between 0° and 15° is almost as good, with respect to minimizing the work of breathing.

Clearly, two angle ranges have emerged as candidates as the optimal angle: 0° to 15° and 60° to 75°. No clear choice between the two can be made based purely on the pulmonary function studies performed thus far and other factors must be considered.

The primary cause of pilot failure is blackout which occurs as a result of inadequate delivery of O_2 to the brain. This may be the result of inadequacy of one or more of the following physiologic phenomenon: 1) pulmonary ventilation, 2) blood-gas communication, and 3) circulation. The first of these is the subject of this dissertation and has brought us to the current dilemma. As to the second, it is known that increased WBA affects the blood and gas portions of the pulmonary system as opposites, i.e., the increased hydrostatic gradient in the circulatory system causes pooling of blood in the lower regions of the lung while, at the same time, it causes pooling of gas in the upper regions, as discussed in Study B. This same study indicates that while the gas is pooling in the upper regions in an upright posture. the best ventilation is occurring in the middle region. This result is interesting when compared to perfusion data obtained by Whinnery[52] who introduced radio-active microspheres into the blood stream of miniature swine undergoing high sustained $+G_z$ acceleration. The microspheres lodged in the pulmonary capillary bed and scintiscanning was used to obtain a "picture" of pulmonary perfusion. His results indicate

that the best perfusion during WBA levels of 2 - 6 G's occurs about half to two-thirds of the way down the lung. This is the same area that our model predicts to be the best ventilated under $+G_z$ acceleration.

Though no data exist in confirmation, it would seem logical that as the angle of attack of the WBA increases toward the supine position and the hydrostatic pressure difference between top and bottom of the lung decreases, perfusion would better distribute blood through the lung just as ventilation does. We are left with the conclusion that an examination of the blood gas communication does not help very much in choosing between the two seat tilt ranges as it seems that the location of the best ventilation and perfusion will match for any seat tilt. It would appear, on the surface, that the 60° to 75° angle would be the best as it allows both ventilation and perfusion to occur over a broader region, but this has not been shown.

The last of the physiological phenomena which may help in choosing the best angle is that of circulation. This is the area that has been most intensely studied and all data points to the same logical conclusion: in the upright position, increased WBA causes blood to pool in the lower extremities and inadequate blood flow to the brain results. Further, an increase in seatback angle toward the prone position relieves the problem. Taking this into consideration we must conclude that the 60° to 75° seat tilt should be optimum in relieving the effects of high sustained WBA.

The studies herein discussed form a basis for what is hoped
will be a long and detailed examination of the high WBA
environment. In the process of determining what may be the
optimum seatback angle for relieving the effects of WBA, we have
developed a data base describing how the lung operates during passive
breathing. This may be used for comparison for future studies.
The model is fully capable of simulating the effects of various
anti-G suits and of different breathing maneuvers such as positive
pressure breathing or the valsalva maneuver. It is also capable
of simulating the effects of WBA on different body types such as
tall or short subjects, slender and husky builds, and obesity.
A long range goal may be to define an optimum subject type
for withstanding WBA.

The model is not limited to the study of the high G
environment. As the study of the effects of high airway resistance
indicates, this model should be very useful in studying various
lung diseases and developing clinical tests for their early
detection and diagnosis.

APPENDIX A: Derivation of Equations

PART I: Alveolar Equations - Table I

Restating the force balance equations (Equations 3, 4, and 5 in the text)   we have

(A-1) $P_{Tx} + P_{bs} = P_{pl} + \overline{P}_g + P_{el}$,

(A-2) $P_{DA} + P_{bs} = P_{pl} + P_{gb} + P_{gAB} + P_{el_{DA}}$,

and

(A-3) $P_j = P_{pl} + P_{g_j} + P_{el_j}$.

Subtracting Equation A-3 from A-1 to eliminate P_{pl} yields

(A-4) $P_j + P_{el_{Tx}} + P_{el_j} = P_{Tx} + P_{bs} - \overline{P}_g + P_{g_j}$.

The resulting equation has been rearranged such that all user defined or constant functions have been grouped on the right.   These we rename

(A-5) $P_{s_j} = P_{Tx} + P_{bs} + P_{g_j} - \overline{P}_g$.

Differentiating Equation A-4 with respect to time, we have

(A-6) $\dot{P}_j + \dfrac{\partial P_{el_{Tx}}}{\partial V_{Tx}} \dot{V}_{Tx} - \dfrac{\partial P_{el_j}}{\partial V_j} \dot{V}_j = \dot{P}_{s_j}$.

(Unless otherwise specified, differentiation will always be assumed to be with respect to time which will be indicated by the dot notation.) Differentiating the equation of state for each alveolar chamber j

yields

(A-7) $\quad \dot{P}_j = \left(\dot{n}_j RT - P_j \dot{V}_j \right) \dfrac{1}{V_j}$.

Solving for V_j from Equations A-6 and A-7 yields

(A-8) $\quad \dot{V}_j = \dfrac{\dfrac{\dot{n} RT}{V_j} + \dfrac{\partial P_{el}_{Tx}}{\partial V_{Tx}} \dot{V}_{Tx} - \dot{P}_{s_j}}{\dfrac{P_j}{V_j} + \dfrac{\partial P_{el}_j}{\partial V_j}}$.

P_{pl} will now be eliminated from Equations A-1 and A-2 such that

(A-9) $\quad P_{el}_{Tx} - P_{el}_{DA} = P_{Tx} - P_{DA} + P_{g b} + P_{g AB} - \overline{P_g}$.

The user defined functions are again on the right and will be renamed

(A-10) $\quad P_{s_2} = P_{Tx} - P_{DA} + P_{g AB} + P_{g b} - \overline{P_g}$.

Differentiating Equation A-9 yields

(A-11) $\quad \dfrac{\partial P_{el}_j}{\partial V_{Tx}} \dot{V}_{Tx} - \dfrac{\partial P_{el}_{DA}}{\partial V_{DA}} \dot{V}_{DA} = \dot{P}_{s_2}$.

Differentiating Equation 2 in the text, the volume equation, gives

(A-12) $\quad \dot{V}_{DA} = \sum\limits_{j=1}^{6} \dot{V}_j - \dot{V}_{Tx}$.

Eliminating $\dot{V}_{DA}$ between Equations A-11 and A-12 and solving for $\dot{V}_{Tx}$

(A-13) $\quad \dot{V}_{Tx} = \dfrac{\dfrac{\partial P_{el}_{DA}}{\partial V_{DA}} \sum\limits_{j=1}^{6} \dot{V}_j + \dot{P}_{s_2}}{\dfrac{\partial P_{el}_{DA}}{\partial V_{DA}} + \dfrac{\partial P_{el}_{Tx}}{\partial V_{Tx}}}$.

The equation for mass balance of an individual gas in the alveoli is a modified form of Equations 11 and 12 in the text such that

(A-14) $\dot{n}_{\ell j} = C_{\ell n} F_{ij} - Diff_{\ell j}$

where the subscript m identifies the chamber, i or j, from which mass is flowing and is dependent on the sign of F_{ij}. Differentiating the equation of state for gas 1 we have

(A-15) $\dot{C}_{\ell j} = (n_{\ell j} - C_{\ell j} \dot{V}_j) \frac{1}{V_j}$

As was stated in the text, water vapor is assumed to be at the saturation point such that if the temperature is constant, C_{wj} is a function of P only, i.e., [46]

(A-16) $C_{wj} = \frac{p_o}{RT} exp\left[\frac{V_L'}{RT} (P_j - P_o) \right]$

where V_L' is the molar volume of water, P_o is a reference pressure and p_o is the vapor pressure of water at P_o. Since

(A-17) $n_{wj} = C_{wj} V_j$

it follows that

(A-18) $\dot{n}_{wj} = V_j \frac{\partial C_{wj}}{\partial P_j} \dot{P}_j + C_{wj} \dot{V}_j$

As $\dot{n}_{wj}$ is not just a function of mass transfer between chambers, a source equation representing evaporation and condensation must be supplied:

(A-19) $\dot{S}_{wj} = C_{wj} \dot{V}_j - C_{wm} F_{ij}$

With the fact in mind that moles of water must be treated differently than the moles of other gasses, we restate the equation of state as

$$(\text{A-20}) \quad P_j = \frac{RT}{V_j} \left(n_{w_j} + n_{T_j} \right)$$

where we define n_{Tj} as

$$(\text{A-21}) \quad n_{T_j} = \sum_{\ell} n_{\ell_j}$$

Differentiating Equation A-20 yields

$$(\text{A-22}) \quad \dot{P}_j = \frac{RT}{V_j} \left[\dot{n}_{w_j} + \dot{n}_{T_j} - \dot{V}_j \left(C_{w_j} + C_{T_j} \right) \right]$$

where

$$(\text{A-23}) \quad C_{T_j} = \sum_{\ell} \frac{n_{\ell_j}}{V_j}$$

Equations A-8, A-13, A-14, A-15, A-18, A-19, and A-22 encompass the equations listed in Table I of the text. This set of equations is severely algebraically coupled. By algebraically coupled it is meant that if each unknown (the set of symbols on the left side of the equations in Table I) is treated as an algebraic variable rather than a differential function, a set of n equations in n unknowns is obtained. This system of equations must be algebraically manipulated until it can be solved sequentially. This was accomplished as follows.

Eliminating $\dot{P}_j$ from equations A-18 and A-22 yields

(A-24) $\dot{n}_{w_j} = \left[X_j \, \dot{n}_{T_j} + \dot{V}_j \left(C_{w_j} - \bar{X} C_j \right) \right] \dfrac{1}{1 - X_j}$

where the following identities are used

(A-25) $X_j = RT \dfrac{\partial C_{w_j}}{\partial P_j}$

and

(A-26) $\bar{C}_j = C_{w_j} + C_{T_j}$.

Further, defining

(A-27) $D_j = C_{w_j} - X_j \bar{C}_j$,

Equation A-24 becomes

(A-28)

Allowing the following identities,

(A-29) $U_j = \dfrac{RT}{V_j \left(\dfrac{P_j}{V_j} + \dfrac{\partial P_{el_j}}{\partial V_j} \right)}$

(A-30) $A_j = \dfrac{\dfrac{\partial P_{el_{Tx}}}{\partial V_{Tx}}}{\dfrac{P_j}{V_j} + \dfrac{\partial P_{el_j}}{\partial V_j}}$

and

(A-31) $B_j = \dfrac{-\dot{P}_{s_j}}{\dfrac{P_j}{V_j} + \dfrac{\partial P_{el_j}}{\partial V_j}}$

Equation A-8 becomes

(A-32) $\dot{V}_j = A_j \dot{V}_{Tx} + U_j \left(\dot{n}_{w_j} + \dot{n}_{T_j} \right) + B_j$

Combining Equations A-28 and A-32 to eliminate $\dot{n}_{wj}$ yields

$$(A-33) \quad \dot{V}_j = \frac{A_j \dot{V}_j + \dfrac{u_j \dot{n}_{Tj}}{1-X_j} + B_j}{1 - \dfrac{u_j D_j}{1-X_j}} \ .$$

Applying the identities

$$(A-34) \quad \gamma_j = \frac{A_j}{1 - \dfrac{u_j D_j}{1-X_j}}$$

and

$$(A-35) \quad \omega_j = \frac{\dfrac{u_j \dot{n}_{Tj}}{1-X_j} + B_j}{1 - \dfrac{u_j D_j}{1-X_j}}$$

to equation A-33, we have the much simpler equation

$$(A-36) \quad \dot{V}_j = \gamma_j \dot{V}_{Tx} + \omega_j$$

   Finally, substituting the identities

$$(A-37) \quad E = \frac{\dfrac{\partial P_{el\,DA}}{\partial V_{DA}}}{\dfrac{\partial P_{el\,DA}}{\partial V_{DA}} + \dfrac{\partial P_{el\,Tx}}{\partial V_{Tx}}}$$

and

$$(A-38) \quad F = \frac{P_{S_2}}{\dfrac{\partial P_{el\,DA}}{\partial V_{DA}} + \dfrac{\partial P_{el\,Tx}}{\partial V_{Tx}}}$$

into equations A-13 gives us

$$(A-39) \quad \dot{V}_{Tx} = E \sum_{j=1}^{6} \dot{V}_j + F \ .$$

Combining Equations A-36 and A-39 to eliminate $\dot{V}_j$ yields

$$(A-40) \quad \dot{V}_{T_x} = \frac{E \omega_T + F}{1 - E \delta_T} \quad ,$$

where we make use of the identities

$$(A-41) \quad \omega_T = \sum_1 \omega_j$$

and

$$(A-42) \quad \delta_T = \sum_1 \delta_j \quad .$$

The system of equations listed in Table I may now be solved using the set of sequential equations listed in Table IV.

ALVEOLAR EQUATIONS

1. $\dot{n}_{\ell_j} = C_{\ell m} F_{ij} - Diff_{\ell_j}$

2. $\dot{V}_{Tx} = \dfrac{E \omega_T + F}{1 - E \gamma_T}$

3. $\dot{V}_j = \gamma_j \dot{V}_{Tx} + \omega_j$

4. $\dot{n}_{\omega_j} = \left(x_j \dot{n}_{T_j} + \dot{V}_j D_j \right) \dfrac{1}{1 - x_j}$

5. $\dot{P}_j = \dfrac{RT}{V_j} \left[\dot{n}_{\omega_j} + \dot{n}_{T_j} - \dot{V}_j \left(C_{\omega_j} + C_{T_j} \right) \right.$

6. $\dot{C}_{\ell_j} = \left(\dot{n}_{\ell_j} - C_{\ell_j} \dot{V}_j \right) \dfrac{1}{V_j}$

7. $\dot{C}_{\omega_j} = \dfrac{\partial C_{\omega_j}}{\partial P_j} \dot{P}_j$

8. $\dot{S}_{\omega_j} = \dot{n}_{\omega_j} - C_{\omega_j m} F_{k_j}$

Where:

1. $\dot{n}_{T_j} = \sum_\ell n_{\ell_j}$

2. $C_{T_j} = \sum_\ell C_{\ell_j}$

3. $x_j = RT \dfrac{\partial C_{\omega_j}}{\partial P_j}$

4. $\overline{C}_j = C_{\omega_j} + C_{T_j}$

5. $D_j = C_{\omega_j} - x_j \overline{C}_{T_j}$

6. $U_j = RT \Big/ \left(\dfrac{P_j}{V_j} + \dfrac{\partial P_{el_j}}{\partial V_j} \right)$

7. $A_j = \dfrac{\partial P_{el_{Tx}}}{\partial V_{Tx}} \Big/ \left(\dfrac{P_j}{V_j} + \dfrac{\partial P_{el_j}}{\partial V_j} \right)$

8. $B_j = P_{s_j} \Big/ \left(\dfrac{P_j}{V_j} + \dfrac{\partial P_{el_j}}{\partial V_j} \right)$

9. $\gamma_j = A_j \Big/ \left(1 - \dfrac{U_j D_j}{1 - x_j} \right)$

10. $\omega_j = \left(\dfrac{U_j \dot{n}_{T_j}}{1 - x_j} + B_j \right) \Big/ \left(1 - \dfrac{U_j D_j}{1 - x_j} \right)$

11. $F = \dot{P}_{s_1} \Big/ \left(\dfrac{\partial P_{el_{DA}}}{\partial V_{DA}} + \dfrac{\partial P_{el_{Tx}}}{\partial V_{Tx}} \right)$

12. $E = \dfrac{\partial P_{el_{DA}}}{\partial V_{DA}} \Big/ \left(\dfrac{\partial P_{el_{DA}}}{\partial V_{DA}} + \dfrac{\partial P_{el_{Tx}}}{\partial V_{Tx}} \right)$

13. $\omega_T = \sum_j \omega_j$

14. $\gamma_T = \sum_j \gamma_j$

TABLE IV

PART II: Airway Equations - Table II

Since volumes in the airway chambers are assumed constant, the derivative of the equation of state for gas is

$$(A\text{-}43) \quad \dot{P}_1 = \frac{RT}{V_1} \left(\dot{n}_{w_1} + \dot{n}_{T_1} \right).$$

The mass balance equation is just Equation 12 in the text.   The derivative of the concentration equation for gas 1 and water vapor w will be

$$(A\text{-}44) \quad \dot{C}_{\ell_1} = \frac{\dot{n}_{\ell_1}}{V_1}$$

$$(A\text{-}45) \quad \dot{C}_{w_1} = \frac{\partial C_{w_1}}{\partial P_1} \dot{P}_1 .$$

The molar values of water in each chamber will then be defined by the equation

$$(A\text{-}46) \quad \dot{n}_{w_1} = V \dot{C}_{w_1}$$

and the source equation

$$(A\text{-}47) \quad \dot{S}_{w_1} = \dot{n}_{w_1} - \left[\sum_{k} n_{w_k} F_{kj} - n_{w_j} F_{jj} \right].$$

Clearly the only coupling between these equations is between Equations A-43, A-45, and A-46.   Substituting Equation A-46 into A-43 to eliminate $\dot{n}_{wj}$ yields

$$(A\text{-}48) \quad \dot{P}_1 = \frac{\dot{n}_{T_j}}{V_1 \left(\frac{1}{RT} - \frac{\partial C_{w_1}}{\partial P_1} \right)} .$$

Thus, we have the set of equations given in Table II which may be solved sequentially.

PART III: Spirometer Equations - Table III

Both pressure and temperature in the spirometer are assumed constant. The temperature, however, is not the same as that in the lungs and will be designated T_s. From the equation of state for gas, we have

(A-49) $\qquad \dot{V}_1 = RT_s \left(n_{w_1} + n_{T_1} \right)$

From the mass balance equation, we have the following set of equations:

(A-50) $\qquad n_{w_1} = C_{w_1} \dot{V}_1$,

(A-51) $\qquad n_{\ell_1} = -C_{\ell m} F_{12}$,

(A-52) $\qquad C_{\ell_1} = \dfrac{1}{V_1} \left(\dot{n}_{\ell_1} - C_{\ell_1} \dot{V}_1 \right)$,

and

(A-53) $\qquad \dot{S}_{w_1} = \dot{n}_{w_1} - C_{wm} F_{12}$.

These equations may be decoupled by combining Equations A-49 and A-50 to yield

(A-54) $\qquad \dot{V}_1 = \dfrac{\dot{n}_{T_1}}{\dfrac{P_1}{RT_s} - C_{w_1}}$.

These equations may now be solved sequentially as listed in Table III.

APPENDIX B: Stability Test

Within the context of finite integration a differential equation (DE) is convergent if the solution to the finite difference equation representing it approches the true solution to the DE as the independent variable step size approches zero. The necessary and sufficient conditions for convergence are that the DE be both a) consistant and b) stable. Consistancy indicates that the finite difference procedure employed does infact represent the DE in question and not some other. Consistancy is usually assumed and is only examined if the equation fails to converge thou it proves stable.

Stability proves to be the more common convergence problem. Inherent to any finite difference approximation of a DE is some degree of error including truncation error and round off error. There exists an upper limit on the independent variable step size below which these errors will not accumulate over a number of integration steps, in which case the equation is said to be stable, and above which they will, causing instability. It should be noted that stability does not indicate that the error will be small - only whether or not it will be amplified.

The equation being examined is the ordinary differential equation (ODE) for pressure in the airways, which in its most general form is

$$(B\text{-}1) \quad \dot{P_j} = \frac{RT}{V_j} \left[\sum_i C_i F_{ij} - C_j \sum_k F_{jk} \right]$$

No convenient technique has yet been developed for the testing

of stability of the ODE though several methods have been developed

for the partial DE (PDE). It now becomes a problem of represent-

ing Equation B-1 in the form of a PDE.

If we assume for simplicity that there is but one Chamber i

and one Chamber j and if we examine Equation B-1 at time t using

step size Δt the finite difference equation would be

$$(B-2) \quad \frac{P_j^{t+\Delta t} - P_j^t}{\Delta t} = \frac{RT}{V_j} \left[F_{ij} \, C_i^t - F_{jk} \, C_j^t \right]$$

where we have chosen to use the concentrations at the current time, t ,

in the approximation. Recalling that concentration is a function of

pressure this becomes

$$(B-3) \quad \frac{P_j^{t+\Delta t} - P_j^t}{\Delta t} = \frac{1}{V_j} \left[F_{ij} \, P^t - F_{jk} \, P_j^t \right] .$$

Now, if the location of chamber j is x and Chamber i is

(x $- \Delta$x) , Equation B-3 is a difference analogue for the PDE

$$(B-4) \quad \frac{\partial P(t,x)}{\partial t} = \frac{-\Delta x}{V_j} \, \frac{\partial P(t,x)}{\partial t} .$$

A stability test that examines the PDE was developed by O'Brien,

et. al.,[48] and has since been treated in numerous numerical methods

texts. The treatment outline advanced by Carnahan, et. al.,[38]

was used to examine Equation B-3. One assumes that a seperation of

variables may be made on the function P(t,x) and that the space

dependent function may be expanded in a Fourier expansion. A specific

solution may then be chosen from the Fourier expansion and substituted

back into the PDE. By defining the amplification factor f represented as

(B-5) $\quad f = \dfrac{T(t + \Delta t)}{T(t)}$

where T(t) is the time dependent part of P(t,x), and where the condition for stability is

(B-6) $\quad f^2 \le 1$

the upper limit of the independent variable Δt may be determined.

When this procedure was applied to Equation B-3, it was found that Δt must be less than zero, which was impossible, indicating that this particular finite difference approximation was absolutely unstable. Other approximations were attempted but none could be found which yielded stability under satisfactory conditions.

1. Burton, R.E., W.F. Storm, L.W. Johnson, S.D. Leverett, Jr. and B.O. Hartman, Stress response of pilots flying high performance aircraft during aerial combat maneuvers, Review of Air Force Sponsored Basic Research in Environmental and Acceleration Physiology, (1976). Wright-Patterson AFB, Ohio.

2. Wunder, C.S., B. Duling and H. Bengele, Gravity as a biological determinant, In: Hypodynamics and Hypogravics. Michael McCally, Academic Press, New York (1968).

3. Gauer, O.Y., Historical aspects of gravitational stress, In: Gravitational Stress in Aerospace Medicine, O.H. Gauer and G.D. Zuidema, Little-Brown, Boston (1961).

4. Suwa, K. and Bendixen, H.H., Pulmonary gas exchange in the tidally ventilated single alveolus model, J. Appl. Physiol., 32: 834 (1972).

5. Scheid, P. and Piiper, J., Analysis of test gas washout from lungs with varying tidal volume; theory, J. Appl. Physiol., 31: 834 (1972).

6. Fry, D.L. and R.E. Hyatt, Pulmonary mechanics: A unified analysis of the relationship between pressure, volume and gasflow in the lungs of normal and diseased human subjects, J. Amer. Med., 29: 672 (1960).

7. Collins, R.E., R.W. Kilpper and D.E. Jenkins, A mathematical analysis of mechanical factors in the forced expiration, Bull. of Mathematical Biophysics, 29, 737 (1967).

8. Gomez, D.M., A physico-mathematical treatment of the distribution of specific tidal volume throughout the lung, Fed. Proc., 21: 439 (1962).

9. Gomez, D.M., A mathematical treatment of the distribution of specific tidal volume throughout the lung, Proc. Nat. Acad. Sci., 49: 312 (1963).

10. Gomez, D.M., W.A. Briscoe and G. Cumming, Continuous distribution of specific tidal volume throughout the lung, J. Appl. Physiol., 19: 683 (1964).

11. Gomez, D.M., A physico-mathematical study of lung function in normal subjects and in patients with obstructive pulmonary disease, Med. Thorac., 22: 275 (1965).

12. Peslin, R., S. Dawson and J. Mead, Analysis of multicomponent exponential curves by the post-widders equation, J. Appl. Physiol., 30: 462 (1971).

13. Saidel, G.M., T.C. Militano and E.H. Chester, Pulmonary gas transport characterization by a dynamic model, Resp. Physiol., 12: 305 (1971).

14. Saidel, G.M., T.C. Militano and E.H. Chester, Mass-balance model of pulmonary oxygen transport, IEEE Trans. (BioMed. Engr.) BME-19: 205 (1972).

15. West, J.B., Ventilation-perfusion inequality and overall gas exchange in computer models of the lung, Resp. Physiol., 1: 88 (1969).

16. West, J.B., Causes of carbon dioxide retention in lung disease, New Eng. J. Med., 284: 1232 (1971).

17. West, J.B., Gas exchange when one lung region inspires from another, J. Appl. Physiol., 30: 479 (1971).

18. Mead, J., T. Taskashimo and D. Leith, Stress distribution in lungs; a model of pulmonary elasticity, J. Appl. Physiol., 28: 596 (1970).

19. Lambert, R.K. and T.A. Wilson, A model for the elastic properties of the lung and their effect on expiratory flow, J. Appl. Physiol., 34: 34 (1973).

20. Grimby, G., T. Takishimo, W. Grahm, P. Macklem and J. Mead, Frequency dependence of flow resistance in patients with obstructive lung disease, J. Clin. Invest., 47: 1455 (1968).

21. Hilberman, M., R.W. Stacy and R.M. Petcos, A phase method of calculating respiratory mechanics using a digital computer, J. Appl. Physiol., 32: 535 (1973).

22. Kilpper, R.W., Analysis of a Continuous, Elastic Single-Chambered Model of the Mammalian Lung, Dissertation, U. of Houston, Texas (1967).

23. Hyatt, R.E. and L.F. Black, The flow-volume curve, a current perspective, Am. Rev. Resp. Dis., 107: 191 (1973).

24. Calvert, R.E., Mathematical Development of a Comprehensive Model of the Human Pulmonary System: Mechanics and Ventilation, Dissertation, U. of Houston, Texas (1967).

25. Gray's Anatomy, 35th British Edition. R. Warwick and P.L. Williams, W.B. Saunders Co., Inc., Philadelphia (1973).

26. Morphometry of the Human Lung. E.R. Weibel, Springer, Berlin (1963).

27. The Pathology of Emphysema. L. Reid, Lloyd-Luke, London (1967).

28. Baker, L.G., J.S. Vetman and R.A. Rhoades, Simultaneous gas flow and diffusion in a symmetric air system; A mathematical model, Respir. Physiol., 21: 119 (1974).

29. Weibel, E.R. and J. Gil, Structure function relationships at the alveolar level, In: Bioengineering Aspects of the Lung. J.B. West, Marcel Dekker, Inc., New York (1977).

30. The Lung; Clinical Physiology and Pulmonary Function Tests. Comroe, Jr., J.H., R.E. Forster II, A.B. DuBois, W.A. Briscoe and E. Carlsey, Year Book Medical Pub., Inc., Chicago (1962).

31. Glazier, J.B., J.M.B. Hughes, J.E. Maloney and J.B. West, Vertical gradient of alveolar size in lungs of dogs frozen intact, J. Appl. Physiol., 23: 694 (1967).

32. Agostoni, E., E. D'Angelo and M.V. Bonanni, The effect of abdomen on the vertical gradient of pleural surface pressure, Respir. Physiol., 8: 332 (1970).

33. D'Angelo, E., M.V. Bonanni, S. Michelini and E. Agostoni, Topography of the Pleural surface pressure in rabbits and dogs, Respir. Physiol., 8: 204 (1970).

34. Agostoni, E. and E. D'Angelo, Topography of pleural surface pressure during simulation of gravity effects on abdomen, Respir. Physiol., 12: 102 (1971).

35. Pedley, T.J., R.C. Schroter and M.F. Sudlow, Gas flow in the airways, In: Bioengineering Aspects of the Lung. J.B. West, Marcel Dekker, Inc., New York (1977).

36. Donachi, R.P., Digital program for water network analysis, J. of Hydrawlics Division (ASCE), 100: 393 (1974).

37. Applied Numerical Methods. B. Carnahan, H.A. Luther and J.O. Wilkes, John Wiley and Sons, Inc., New York (1969).

38. Methods for the Numerical Solution of Partial Differential Equations. D.U. Von Rosenberg, American Elsevier Publishing Co., Inc., New York (1975).

39. Rohrer, F., Der stromungswiderstand in den menschlichen atemwegen und der einfluss der unregelmassigen verzweigung des bronchialsystems auf den atmungsverlauf in verschiedenen lungenbezirden, Arch. ges. Physiol., 162: 225 (1915).

40. Rohrer, F., Der zusmmenhang der atemkrafte und ihre abhangigkeit vom dehnumgszustand der atmungsorgane, Arch. ges. Physiol., 165: 419 (1925).

41. Rohrer, F., K. Nakasone and K. Wirz, Physiologie der Atembe Wegung Handbuch der Normalen und Pahologischen, II, Berlin, Springer (1925).

42. Flow of Fluids through Porous Materials. R. E. Collins, The Petroleum Publishing Co., Tulsa, Okla. (1976).

43. D. E. Jenkins, Unpublished research, Baylor College of Med., Houston, TX. (1976).

44. Hoppin, F.G.,Jr. and J. Hildebrandt, Mechanical properties of the lung, In: Bioengineering Aspects of the Lung. J.B. West, Marcel Dekker, Inc., New York (1977).

45. Gray's Anatomy, 35th British Edition. R. Warwick and P.L. Williams, W.B. Saunders Co., Inc., Philadelphia (1973).

46. Hyatt, R.E., Schilder, D.P. and D.L. Fry, Relationship Between Maximum Expiratory Flow and Degree of Lung Inflation, J. Appl. Physiol., 13 331 (1958).

47. Gell, D.F. and H.N. Hunter, Phy:iological investigation of increasing re⁻istance to blackout by progre.sive backward tilting to the supine position, <u>J. Aviat. Med</u>., <u>25</u>: 568 (1954).

48. Crossley, R.J. and D.H. Glaister, Effects of posture on tolerance to positive (+Gz) acceleration, <u>AGARD CP-82</u>, Item 6 (1971).

49. Burns, J.W., Re-evaluation of a tilt-back seat as a means of increasing acceleration tolerance, <u>Aviat. Space Environ. Med</u>., <u>46</u>: 55 (1975).

50. Agostoni, E., Statistics of the respiratory system, In: <u>The Respiratory Muscles</u>. E.J.M. Campbell, E. Agostoni and J. Newsom Davis, W.B. Saunders Co., Philadelphia (1970).

51. <u>The Effects of Gravity and Acceleration on the Lung</u>. D.H. Glaister, Advisory Group for Aerospace Research and Development (AGARD). NATO, England (1970).

52. Whinnery, J.E. and M.H. Laughlin, The effects of G_z acceleration on pulmonary perfusion in the miniature swine, <u>Review of Air Force Sponsored Basic Research in Environmental and Acceleration Physiology</u>, St. Louis, Missouri (1979).

53. Ingram, Jr., R.H., C.F. O'Cain, Frequency dependence of compliance in apparently healthy smokers versus non-smokers, <u>Bull. Physiol. and Pathol. Resp</u>., <u>7</u>: 195 (1971).